8-2021

Foliar Photodegradation in Pesticide Environmental Modeling

Sean M. Lyons
Utah State University

FOLIAR PHOTODEGRADATION IN PESTICIDE ENVIRONMENTAL MODELING

by

Sean M. Lyons

A thesis submitted in partial fulfillment

of the requirements for the degree

of

MASTER OF SCIENCE

in

Chemistry

Approved:

_____	_____
Kimberly J. Hageman, Ph.D.	Steven I. Scheiner, Ph.D.
Major Professor	Committee Member
_____	_____
Robert S. Brown, Ph.D.	D. Richard Cutler, Ph.D.
Committee Member	Interim Vice Provost
	of Graduate Studies

UTAH STATE UNIVERSITY

Logan, Utah

2021

ABSTRACT

Foliar Photodegradation in Environmental Modeling

by

Sean Lyons, Master of Science

Utah State University, 2021

Major Professor: Kimberly Hageman, Ph.D.
Department: Chemistry & Biochemistry

Pesticide fate models are one tool that could help to maintain the benefits of pesticide use while minimizing the adverse effects. Several models exist that predict several processes impacting pesticide dissipation, including volatilization, photodegradation, wash-off, and foliar penetration. One area these models currently fall short is in the photodegradation component. Photodegradation will be specific to the chemical as well as the light conditions, yet these models use a constant, generic rate for all chemicals in all conditions due to the limited amount of data focused on pesticide photodegradation on leaves.

With the goal of improving the photodegradation component in pesticide fate modeling, I developed the Pesticide Dissipation from Agricultural Land (PeDAL). Building off the pre-existing volatilization module, the Pesticide Loss via Volatilization (PLoVo) model, I incorporated foliar photodegradation by combining reported kinetics data from the literature with Bird's Clear Sky Model, which can predict hourly sunlight intensities for any location on Earth. A generic foliar penetration component was also included in the PeDAL model. Dissipation studies described in the literature were simulated using the PeDAL model. Comparing modeled versus measured times

for the pesticide concentration to dissipate to half of its concentration immediately following application (DT_{50}) showed that the PeDAL model could accurately describe pesticide dissipation. Sensitivity analyses were then conducted on the photodegradation component of the model and it was used to predict pesticide emission flux, which could be used in atmospheric transport models, and to examine the influence of application timing on pesticide dissipation.

Due to the limited number of foliar pesticide photodegradation rates reported in the literature, the PeDAL model is limited in its use. I conducted a series of experiments with a solar simulator to measure pesticide photodegradation rates on alfalfa leaves. The active ingredients chlorpyrifos, lambda-cyhalothrin, and indoxacarb were tested as pure active ingredient and part of a commercial formulation. Chlorpyrifos exhibited no photodegradation, supporting previous data suggesting photodegradation is a minor dissipation pathway for chlorpyrifos. Lambda-cyhalothrin had pseudo-first order rate constants of 0.042±0.017 h^{-1} and 0.056±0.018 h^{-1} for the active ingredient and formulation, respectively. Indoxacarb degraded at 0.035±0.018 h^{-1} and 0.037±0.21 h^{-1}.

(122 pages)

PUBLIC ABSTRACT

Foliar Photodegradation in Pesticide Environmental Modeling

Sean Lyons

The work described here was conducted to better understand how pesticides will behave following their application to crops or soil. This understanding will allow for better use of pesticides which will protect the environment and non-target organisms while remaining effective against pests. The Pesticide Dissipation form Agricultural Land (PeDAL) model was developed to simulate pesticide behavior following application and laboratory experiments focused on the photodegradation of select pesticides on alfalfa leaves were conducted to support this model.

ACKNOWLEDGMENTS

First, I would like to thank my advisor, Dr. Kimberly Hageman, for her support and guidance over the past three years. You have helped greatly in making my experience at USU as enriching and successful as I would like to think it has been.

To my fellow Hageman Group members, Ashlie, Jeffrey, Calvin, Rob, Shan, and Ruiwen, thank you all so much for your help. From helping with instrument maintenance, sample collection, improving papers and presentations, and just about everything else, you all have been invaluable in me completing the various projects I was involved in.

To my other committee members, Dr. Brown and Dr. Scheiner, the courses I took with Funding related to this project came from the United States Department of Agriculture (USDA) National Institute of Food and Agriculture (NIFA).

you as well as your support and guidance during divisional seminar helped to improve the quality of my work and my knowledge as a chemist.

I would like to thank our collaborators, Dr. Scott Bernhardt, Dr. Ricardo Ramirez, and Dr. Theresa Pitts-Singer for supplying me with the pesticide formulations and alfalfa leaves I needed for my research.

Thank you to Dr. Casey Simons for his assistance on various aspects of my research. Thank you to Dr. Thomas Borch (Colorado State University) for allowing me the opportunity to spend one month in his lab so I could gain experience using his solar simulator

Finally, I would like to thank my roommate, Alex, and especially my dog, Lilly, for helping to give me an escape from research when I needed it and for keeping me company outside of the lab during this global pandemic we've found ourselves in.

Sean Lyons

CONTENTS

LIST OF TABLES

Page

LIST OF FIGURES

Page

LIST OF ABBREVIATIONS

Abbreviation	Definition	Units	Default Value
2,4-D	2,4-dichlorophenoxyacetic acid		
A_{field}	Area of field	m^2	10,000
a.i.	Active ingredient		
BCSM	Bird's Clear Sky Model		
$c_{i,air\text{-}boundary(plant)}$	Concentration of chemical 'i' in plant-air boundary layer at equilibrium	$g\ L^{-1}$	
$c_{i,air\text{-}boundary(soil)}$	Concentration of chemical 'i' in soil-air boundary layer at equilibrium	$g\ L^{-1}$	
$c_{i,air(turbulent)}$	Concentration of chemical 'i' in turbulent air	$g\ L^{-1}$	0
$c_{i,o}$	Concentration of chemical 'i' immediately following application	$g\ L^{-1}$	
$c_{i,t}$	Concentration of chemical 'i' at time 't' after application	$g\ L^{-1}$	
CC	Cloud coverage	%	25
CI	Confidence interval		
CPL_{24h}	Cumulative Percent Loss in 24 h	%	
D_{air}	Air diffusion constant	$m^2\ h^{-1}$	
$d_{air\text{-}boundary(plant)}$	Thickness of plant-air boundary layer	m	
$d_{air\text{-}boundary(soil)}$	Thickness of soil-air boundary layer	m	0.001
$D_{air(T)}$	Air diffusion constant at atmospheric temperature	$m^2\ h^{-1}$	
$D_{air(T,ref)}$	Air diffusion constant at reference temperature (293.15 K)	$m^2\ h^{-1}$	0.0179
DDT	Dichloro-diphenyl-trichloroethane		
DT_{50}	Time for half of original pesticide concentration to dissipate	d or h	
EPA	Environmental Protection Agency		
EPI	Estimation Programs Interface		
$F_{i,air\text{-}boundary(plant)}$	Fraction of chemical 'i' in plant-air boundary layer		
$F_{i,air\text{-}boundary(soil)}$	Fraction of chemical 'i' in soil-air boundary layer		
f_{oc}	Fraction of organic carbon	$g\ g^{-1}$	0.02
FOCUS	Forum for the Coordination of pesticide fate models and their Use		
GC	Gas chromatography		
h_{leaf}	Leaf thickness	m	0.0002
$\Delta H_{i,plant\text{-}air}$	Enthalpy associated with the transfer of chemical 'i' from plant phase to air	$J\ mol^{-1}$	
HPLC	High-performance liquid chromatography		
$\%I$	Foliar intercept fraction (% of pesticide that lands on plants)	%	100

I_{act}	Actual intensity of solar radiation experienced in field	W m^{-2}	
I_{BCSM}	Intensity of solar radiation predicted by Bird's Clear Sky Model	W m^{-2}	
I_{ref}	Intensity of solar radiation in reference	W m^{-2}	
IUPAC	International Union of Pure and Applied Chemistry		
$J_{i,plant}$	Volatilization flux of chemical 'i' from plant compartment	mg $m^{-2}h^{-1}$	
$J_{i,soil}$	Volatilization flux of chemical 'i' from soil compartment	mg $m^{-2}h^{-1}$	
$J_{i,total}$	Volatilization flux of chemical 'i' from all compartments	mg $m^{-2}h^{-1}$	
$K_{air\text{-}water}$	Air-water partition coefficient	dimensionless	
$K_{octanol\text{-}air}$	Octanol-air partition coefficient	dimensionless	
$K_{octanol\text{-}water}$	Octanol-water partition coefficient	dimensionless	
$k_{i,pen}$	Penetration rate of chemical 'i' into the leaf	h^{-1}	0.002
$k_{photo(act)}$	Actual photodegradation rate	h^{-1}	
$k_{photo(ref)}$	Reference photodegradation rate	h^{-1}	
$K_{plant\text{-}air}$	Plant-air partition coefficient	dimensionless	
$K_{plant\text{-}air(T)}$	Plant-air partition coefficient at atmospheric temperature	dimensionless	
$K_{plant\text{-}air(T,ref)}$	Plant-air partition coefficient at reference temperature	dimensionless	
$K_{soil\text{-}air}$	Soil-water partition coefficient	dimensionless	
$K_{water\text{-}air}$	Water-air partition coefficient	dimensionless	
LAI	Leaf area index	dimensionless	4.0
l_{leaf}	Leaf length	m	0.10
$m_{i,app}$	Mass of chemical 'i' applied	g	100
$m_{i,pen}$	Mass of chemical 'i' that has penetrated the leaf	g	
$m_{i,photo}$	Mass of chemical 'i' that has undergone photodegradation	g	
$m_{i,plant(av)}$	Mass of chemical 'i' in the plant compartment that is available to undergo photodegradation, volatilization, or penetration	g	
PEARL	Pesticide Emissions at Regional and Local scales		
PELMO	Pesticide Leaching Model		
PeDAL	Pesticide Dissipation from Agricultural Land		
PLoVo	Pesticide Loss via Volatilization		
PNA	p-nitroanisole		
PWP	Percent of water on plant surface relative to volume of plant material	%	25
R	Ideal gas constant	kJ mol^{-1} K^{-1}	0.008314

R^2	Coefficient of determination		
RH	Relative humidity	%	100
RMSE	Root mean square error		
t	Time after application	days (d)	
T	Atmospheric temperature	K	293.15 K
T_{avg}	Average temperature of dissipation study	K	
T_{input}	Input temperature for PeDAL model	K	293.15 K
T_{max}	Maximum atmospheric temperature of dissipation study	K	
T_{ref}	Reference temperature	K	293.15 K
USGS	United States Geological Survey		
$V_{air\text{-}boundary(plant)}$	Volume of plant-air boundary layer	L	
$V_{air\text{-}boundary(soil)}$	Volume of soil-air boundary layer	L	
V_{plant}	Volume of plant phase	L	
V_{soil}	Volume of soil	L	
$V_{water(plant)}$	Volume of water associated with plant surface	L	
$V_{water(soil)}$	Volume of water in the soil compartment	L	
WS	Wind speed	m s^{-1}	2.0

CHAPTER 1: INTRODUCTION

General Background on Pesticides

The term pesticide refers to any chemical, natural or synthetic, that is used to control against a destructive pest. These pests include insects, weeds, and many other organisms and diseases that disrupt the production of food or poses a threat to health and comfort.[1] Given the number of potential pests, pesticide have been a valuable tool for farmers and society as a whole.

In the past pesticides have provided humans protection against disease. The pesticide dichloro-diphenyl-trichloroethane (DDT) was used with great success to help combat the spread of malaria in the middle of the 20th century. DDT was also used for insect control in agricultural and residential settings and aided in combatting other insect-caused diseases such as typhus.[2]

In addition to protecting human health, pesticides are also extremely important for the agricultural industry. By protecting against weeds, pest insects, and disease, pesticides allow for the production of larger, higher-quality yields.[3] This is especially important given the increasing global demand for food caused by the growing human population. In certain crops, pests have been shown to reduce yields by >50%[1] and weeds have exhibited reductions of up to nearly 80% in the yields of dry land crops.[3] However, through the use of pesticides along with higher-yield seeds and improved irrigation systems, food grain production nearly quadrupled from 50 million tons in 1948-1949 to 196 million tons at the end of the century. Similar growth has been seen for the production of wheat in the United Kingdom, corn in the United States, and many other crops throughout the world. Along with this increase in food production is the secondary benefits of improved nutrition that generally arises from eating these fruits and vegetables.[3,4] Increased food production can help to manage malnutrition which is responsible for the deaths of an estimated 12-15 million children every year.[5]

From the perspective of human comfort and leisure, pesticides help to maintain turf on surfaces such as golf course and other sports fields and are even included in many items traditionally found in homes.[3,4] For example, fungicides are often included in many items, such as plastics, paints, and caulks, to prevent mold from growing. For many of the reasons mentioned above, pesticides are often used in supermarkets and in homes to manage pests, protect food supplies, and increase human comfort.[1]

The economic benefits of pesticide usage cannot be understated and are linked with the benefits already mentioned. With increased crop yields and thus an increase in the food supply, the prices for consumers stay low. The benefits of reduced crop losses from pesticide usage is estimated to be worth tens of billions of dollars annually to the agricultural industry of the United States alone.[5]

Cooper et al. illustrated a more comprehensive set of the primary and secondary benefits that arise from pesticide usage in Figure 1.[5] Primary benefits are grouped into three areas based the intended use of the pesticide while secondary benefits are grouped based on if the benefit applies to the local, national, or global scale. Links between primary and secondary benefits are established with lines connecting them in the Figure 1.

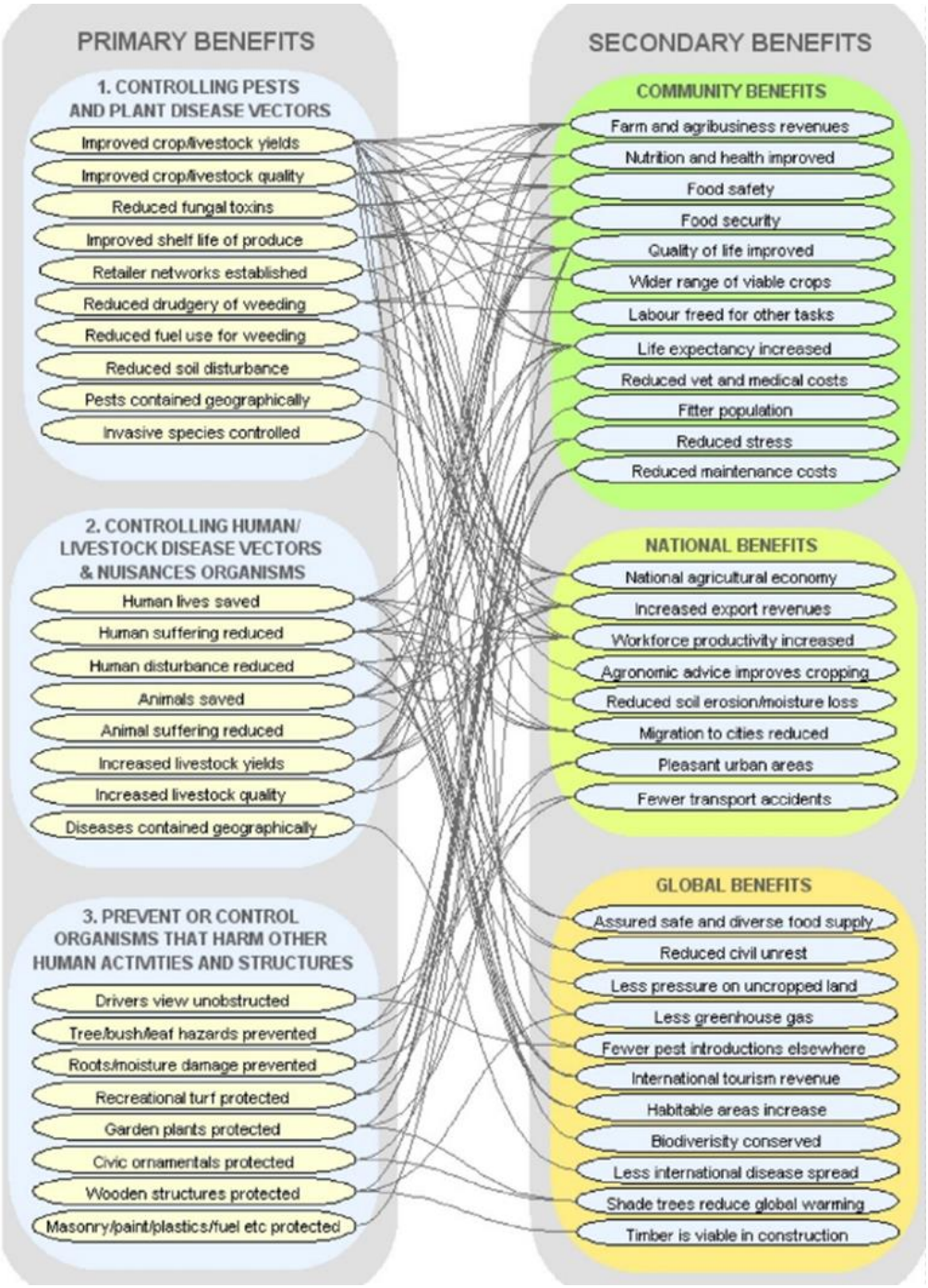

Figure 1. Primary and Secondary Benefits of Pesticide Usage[5]

Given this wide range of benefits, substantial pesticide usage is expected. The U.S. Environmental Protection Agency (EPA) reported that in 2012, the global usage of pesticides totaled nearly 3 billion kilograms with the United States responsible for about 20% of the total usage. Within the U.S., the agricultural industry comprised just under 90% of the total usage with household usage and other commercial/industrial applications accounting for the remainder.[6]

This widespread usage of pesticides becomes controversial when considering their adverse effects on the environment, human health and other organisms. When pesticides reach non-target areas or organisms, the benefits are quickly replaced with negative outcomes.[1,3,4,7] Indiscriminate use of pesticides can also result in the development of pest resistance. Resistance decreases the efficacy and thus the benefits of pesticide use while continuing to pose a threat to the health of the environment and exposed humans and other organisms.[8]

Pesticides contaminate a variety of matrices, including soil, vegetation, surface water, ground water, and the atmosphere, and the extent of this contamination is nearly universal. A United States Geological Survey (USGS) study examining the water quality in river basins throughout the country reported over 90% of samples were contaminated with at least one pesticide, if not multiple.[3] A similar study in India examining the ground water used in wells reported that 58% of the drinking water samples analyzed had concentrations for organochlorine pesticides exceeding the EPA recommendation.[3]

Soil, which in some cases may even be the target matrix, can also be negatively impacted by the presence of pesticides. Pesticide usage can reduce populations of microorganisms, like bacteria and fungi, which are vital for plant growth through their roles in the nitrogen cycle and nutrient profile of soil.[3] Similarly, earthworms who have been exposed to pesticides has resulted in reduced masses in earthworm populations and decreased reproduction.[9] Like bacteria and fungi, earthworms provide benefits to the soil by increasing the amount of air and water that can get into the soil as well as breaking down organic materials into forms that can be used by plants.[10] Given

the importance of soil to crop production, the impacts that pesticides have on essential soil organisms must be not be overlooked.

Spray drift is a consequence of pesticide application and results in a portion of the application never landing on its intended target. Depending on the meteorological conditions and the equipment being used, spray drift can account for losses in application mass ranging from 2-25%.[3] Atmospheric transport following pesticide volatilization can similarly result in pesticide moving through the atmosphere and reaching non-target areas. Both of these processes can be very damaging if the pesticide lands on vegetation it wasn't intended for, particularly in the case of herbicides. Plant damage caused by unintended pesticide exposure includes the herbicide glyphosate reducing seed quality and increasing susceptibility to disease, the herbicide clopyralid reducing yields in potato crops, and phenoxy herbicides causing damage to nearby trees and shrubs. There are many more examples of these types of negative consequences from unintended exposure including the herbicide glyphosate which the EPA considers a threat to dozens of endangered plant species.[3] Further complicating the use of pesticides is that the process of atmospheric transport can carry pesticides thousands of miles to remote areas and areas where these chemicals have never been used.[11,12] This results in the contamination of high-latitude or high-elevation locales that would otherwise be thought of as pristine.

This ubiquitous contamination of the environment and resulting exposure to humans and other organisms is associated with a long list of maladies. Studies have shown certain pesticides like trifluralin are highly toxic to fish and can cause deformities in their vertebrae.[3] Similar results have been shown in studies examining other studies. Sub-lethal effects in fish and insects have also been shown from pesticide exposure.[3,4,13] Neonicotinoids, a commonly used class of pesticides, has been shown to have negative impacts on bees and is thought to have some role in Colony Collapse Disorder being observed recently.[14,15] Exposure to neonicotinoids has also been

linked to physiological and reproductive issues in deer in Montana and South Dakota suggesting that this class of chemicals could have adverse effects on a wide range of organisms.[16]

Humans also experience adverse effects after pesticide exposure with a large set of data supporting this relationship. To briefly highlight some of these exposure side effects, DDT and other organochlorine pesticides have been linked with endocrine disorders and negative impacts on embryonic development and lipid metabolism among others.[7] Exposure to chlorpyrifos, an organophosphate pesticide, has been associated with neurological issues in children including decreased IQ.[17] Serious health effects on the cardiovascular, reproductive, and nervous systems have also been associated with exposure to other organophosphate pesticides as well as increased risk for dementia.[7] The list of negative health consequences from pesticide exposure could go on and on.

One way to attempt to curtail these effects is through regulation. For example, the U.S. EPA issued a series of guidelines restricting the use of DDT beginning in the late 1950s and into the 1960s. In 1973, the U.S. Court of Appeals supported the EPA's ban on DDT which faces opposition from the pesticide industry.[18] While regulation can be well-intended, the case of DDT highlights the problems with relying solely on regulation. Passing the necessary legislation generally takes a very long time and usually only occurs after adverse effects have already been observed. Despite some scientists raising concerns as early as the 1940s, the use of DDT and its impacts on the environment didn't receive much attention until 1962 when Rachel Carson published her book *Silent Spring*, highlighting many of the adverse effects associated with widespread pesticide usage.[18] And even after publishing this work, it still took 11 years for DDT to be banned. Chlorpyrifos, originally designed as a less persistent alternative to DDT, is another example of the limits of relying on regulation. The association between chlorpyrifos exposure and neurological issues in children led to a ban on most household uses of the product in 2000, however, very little was done for the ensuing two decades following this restriction being adopted. The use

of the pesticide did slowly decline over time after the restriction was put in place, but that still resulted in about 2000 metric tons of chlorpyrifos being applied in the United States annually by 2016.[17] This is still a substantial amount given chlorpyrifos's semi-volatile nature and ability to undergo atmospheric transport. The case of chlorpyrifos also illustrates the bipartisan nature of attempting to pass regulations with differences in policy and enforcement arising in the EPA as the presidency shifted from the Obama administration to the Trump administration.[17] Due to the reactionary nature of pesticide regulations along with the politics and time associated with it, regulatory action isn't enough to alleviate the negative outcomes of pesticides.

Pesticide Dissipation and Environmental Modeling

A second option to mitigate the negative impacts of pesticide use is through a better understanding of pesticide fate following application. With a better understanding of the processes

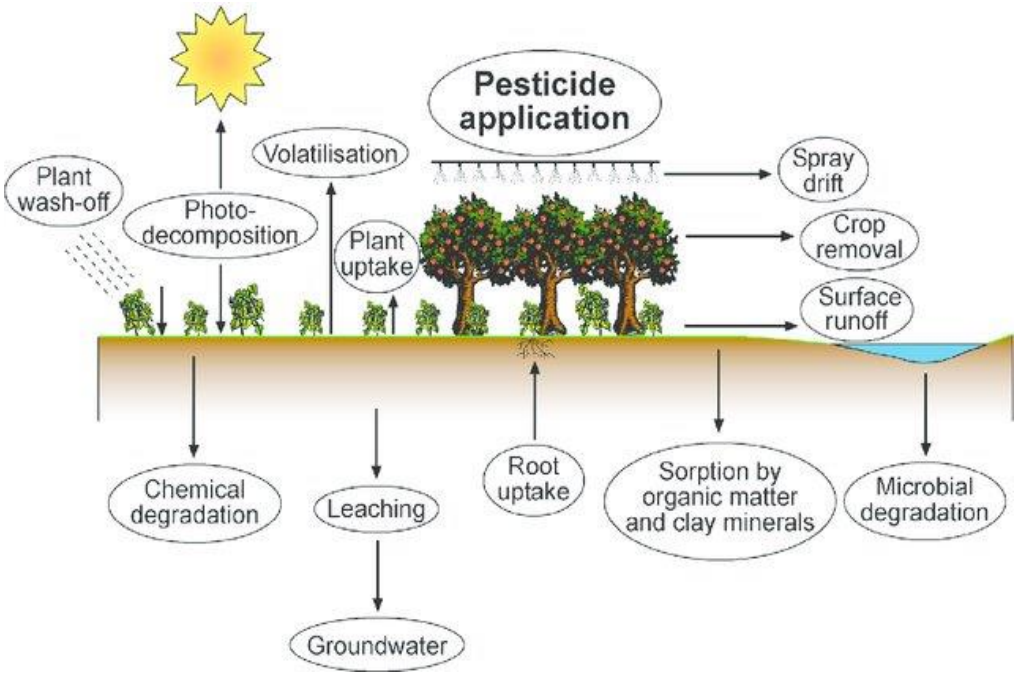

Figure 2. Environmental Processes Impacting Pesticide Fate Following Application[19]

that impact a chemical in the environment, applicators could make more informed decisions about their usage. With accurate predictions of post-application fate, the benefits of pesticides could be maintained while minimizing the adverse consequences through reductions in mass of pesticide being applied or frequency of applications. However, this is a difficult task due to the complexities of processes impacting a pesticide post-application. Pesticide dissipation, or the reduction in pesticide concentration in a given area, is determined by a variety of processes including volatilization from soil and vegetation (followed by subsequent atmospheric transport), photodegradation, wash-off from leaves or run-off from soil caused by precipitation, foliar penetration, and any other process that the pesticide undergoes. These processes, along with several others that impact pesticide fate, are illustrated in Figure 2.[19]

In addition to accounting for all these processes, the extent that each of these processes impact pesticide dissipation varies wildly depending on the physicochemical properties of the pesticide, the characteristics of the field to which it is applied, and the meteorological conditions to which it is subjected.[20] Past work has been dedicated to understanding some of these processes individually as well as holistically in order to be able to accurately describe pesticide fate.

Pesticide volatilization modules such as the Pesticide Loss via Volatilization (PLoVo) model have been developed previously in the Hageman Research group.[21] Using partition coefficients to describe the interactions between a pesticide and leaf surfaces or soil and Fick's Law of Diffusion, volatilization from soil or plants could be calculated. Modules like PLoVo are valuable because, once they are evaluated and shown to be satisfactory, they allow for an examination of different factors that impact pesticide volatilization in a much cheaper, quicker way than conducting actual field experiments and extracting/analyzing samples. However, with only one process included they lack the ability to fully simulate environmental fate except in the circumstances where volatilization is the only loss process.

Several models have already been developed to better predict pesticide dissipation as a whole including the Pesticide Emission Assessment at Regional and Local scales (PEARL) model[22–24], SURFATM-Pesticides model[25,26], and the Pesticide Leaching Model (PELMO)[27]. These models include the ability to simulate volatilization, foliar photodegradation, foliar penetration, and include a wash-off component. The volatilization component in these models is chemical-specific by using a similar partitioning method as in PLoVo. However, in these models, photodegradation is modeled using a generic photodegradation rate that is not specific to the chemical or the sunlight conditions being experienced. Despite relatively little information being reported in the literature on foliar photodegradation of pesticides, vast differences have already been observed in the photoreactivity of the few pesticides that have been investigated.[28,29] These differences are likely to cause large variations in pesticide dissipation observed in the field and modeling techniques that treat photodegradation as a generic component likely will not produce accurate results. To obtain the best modeling results, future models should be developed with a chemical-specific, location-specific photodegradation component that adjusts for changing light regimes.

Project Objectives

The overall aim of this project was to create a tool that accurately simulates pesticide fate following application to planted fields that can be used by applicators to make more informed pesticide management decisions. Objectives of this thesis project were:

1. Develop an environmental fate model for accurately predicting pesticide dissipation with an improved foliar photodegradation component that is chemical- and location-specific (Chapter 2).

2. Measure photodegradation rates for select pesticides on leaf surfaces that serve as inputs for the environmental fate model (Chapter 3).

Background to Chapter 2

Accurate, reliable environmental fate models could be important tools in improving the efficacy of pesticide applications against target pests and ensuring good crop yields while protecting beneficial insects. Current models exist that include volatilization, wash-off, foliar penetration, and photodegradation. However, the photodegradation component typically used in existing models is a generic, constant rate that is not specific for the pesticide of interest or the changing lighting conditions. To address this area, I developed the pesticide fate model, which has been named the Pesticide Dissipation from Agricultural Land (PeDAL) model. The PeDAL model was built off the framework of an existing module for predicting pesticide volatilization from soil and plants called the Pesticide Loss via Volatilization (PLoVo) model.[21] Volatilization was calculated using partition coefficients and Fick's Law of diffusion while foliar photodegradation was incorporated into the model by combining kinetics data reported in the literature with a module for predicting the hourly sunlight intensity (Bird's Clear Sky Model).[30] This improved upon past approaches for modeling photodegradation by making the calculations for this process chemical and location-specific. A generic foliar penetration component was also included to make the model more realistic. While there is little data available on pesticide penetration into leaves, including a generic penetration component provides a more accurate prediction since pesticide that has penetrated the leaf is unavailable to undergo volatilization or photodegradation.[31]

Chapter 2 describes the development and evaluation of the PeDAL model in more detail. Sensitivity analyses were conducted to highlight the importance and benefits of our new approach

for simulating pesticide photodegradation. Different aspects of pesticide dissipation were then examined using the PeDAL model. This chapter is a modified version of my first-author paper in *Environmental Science & Technology* about the PeDAL model.[32] Modifications were made to include portions of the Supporting Information in the main text to allow for an easier understanding of certain aspects of the model. The only co-author on this paper is Dr. Kimberly Hageman who provided feedback on project design and preparation of the manuscript for publication.

Background to Chapter 3

As is highlighted in chapter 2, pesticide dissipation is heavily influenced by the pesticide's photoreactivity on leaf surfaces. Despite the important role photodegradation plays in overall dissipation and the large variation in pesticide photoreactivity on leaf surfaces that has already been shown, very few pesticides have photodegradation rates available. Further complicating the use of the limited number of available rates is the fact that only a select few are a result of experiments investigating pesticide photodegradation on leaf surfaces. Most are conducted in solutions of organic solvents or glass or use only UV-light. Due to these reasons, the environmental relevance of these studies is limited and thus, the use of this data in the PeDAL model is prohibited.

To increase the number of foliar photodegradation rates in the literature and expand the potential use of the PeDAL model, I conducted laboratory experiments to obtain foliar photodegradation rates for select pesticides. Experiments were conducted using a solar simulator to mimic natural sunlight and I measured photoreactivity for three pesticides (chlorpyrifos, lambda-cyhalothrin, and indoxacarb) on alfalfa leaves. For all pesticides, the pure active ingredient and the chemical as part of a commercial pesticide formulation were examined separately.

This chapter is written in the format of a journal article. This work is unpublished at the moment, but in the future will be combined with data from four field dissipation studies I conducted on alfalfa at the Greenville Research Farm in Logan, UT in spring and summer 2020. The photodegradation experiments along with the field dissipation studies will allow for the PeDAL model to be evaluated and optimized for alfalfa fields.

CHAPTER 2: PEDAL MODEL

Introduction

The effectiveness of a pesticide (insecticide, herbicide, fungicide, etc) on a plant surface is inherently affected by how long it persists on that surface, *i.e.* how quickly it dissipates following application.[33] Pesticide dissipation is governed by the combination of all processes that reduce its concentration on foliage; these include volatilization, photodegradation, microbial degradation, and wash-off. The dissipation rate thus depends on many factors, including the physicochemical properties of the pesticide, the effects of adjuvants in the formulation, meteorological conditions, and the characteristics of the plant to which it is applied.[20] Pesticide dissipation is often expressed in terms of the time required to reach half of the pesticide's concentration immediately after application (DT_{50}).

A number of models for predicting pesticide fate, or certain aspects of pesticide fate, following application to planted fields have been described. For example, the Pesticide Emission Assessment at Regional and Local scales (PEARL) model,[22,23,34] the Pesticide Leaching Model (PELMO),[27] and the SURFATM-Pesticides model[25,26] predict pesticide fate post-application by incorporating volatilization, photodegradation, foliar penetration, and wash-off into their models. In addition to the models described above, Fantke et al. developed a regression-based model for predicting pesticide dissipation based on a statistical analysis of a large data set of measured pesticide half-lives.[35] The Fantke model included parameters related to the chemical substance class (e.g. carbamates, triazoles) and properties, plant type, and air temperature.

With the exception of the Fantke model, the authors of the pesticide fate models described above have indicated that, to at least some degree, chemical- and condition-specific photodegradation rates could also be incorporated into their models. However, only a handful of measured pesticide photodegradation rates on leaf surfaces have been published and the models described above do not include modules for predicting changing photodegradation rates under different light conditions. Instead, users of these models have generally employed a constant, generic photodegradation rate (d^{-1}) that is not specific to the pesticide, location, or conditions.[25,27,34] While this is likely better than not including photodegradation at all, this simplistic approach could clearly result in significant errors in predicted pesticide dissipation rates, especially for extremely photostable or photolabile pesticides. Illustrating the potential for error, current reported foliar photodegradation rates for pesticides range over three orders of magnitude, from 1.37×10^{-3} h^{-1} (at 1000 W m^{-2}) for chlorpyrifos[29] to 0.11 h^{-1} for cycloxydim[28] (at 400 W m^{-2}). To best capture the effects of photodegradation on pesticide dissipation, models should also incorporate the effects of naturally changing light intensities and cloud cover on photodegradation rates. For example, one study reported roughly 90% photodegradation of the organophosphate insecticide Phoxim on tea bushes after 4 hours of exposure on a sunny day versus only 60% degradation for Phoxim applied to bushes in artificial shade.[36,37]

The aim of the study described here was to develop and evaluate an improved approach for incorporating foliar photodegradation rates into pesticide fate models. We accomplished this by compiling measured pesticide-specific photodegradation rates on leaf surfaces from the literature and developing an hourly light-intensity adjustment factor for these rates. We used this approach in a new pesticide fate model that we introduce here called the Pesticide Dissipation from Agricultural Lands (PeDAL) model. The PeDAL model was designed to predict pesticide DT_{50} values, as well as pesticide emission rates to air, following application. The emission rates can be combined with dispersion models, e.g. SCREEN3,[38] to predict pesticide concentrations in air. The

PeDAL model incorporates pesticide photodegradation from leaf surfaces, volatilization from vegetation and/or soil, and foliar penetration (Figure 3). The photodegradation rates used in the PeDAL model are specific to the chemical and are adjusted for location and solar intensity; pesticide volatilization is calculated using the approach used in the Pesticide Loss via Volatilization (PLoVo) model.[21]

To evaluate the PeDAL model, we compiled a list of measured DT_{50} values, as well as the reported field and meteorological conditions obtained during the measurements, from a variety of experiments described in the literature. We used DT_{50} values for 6 pesticides from 49 different

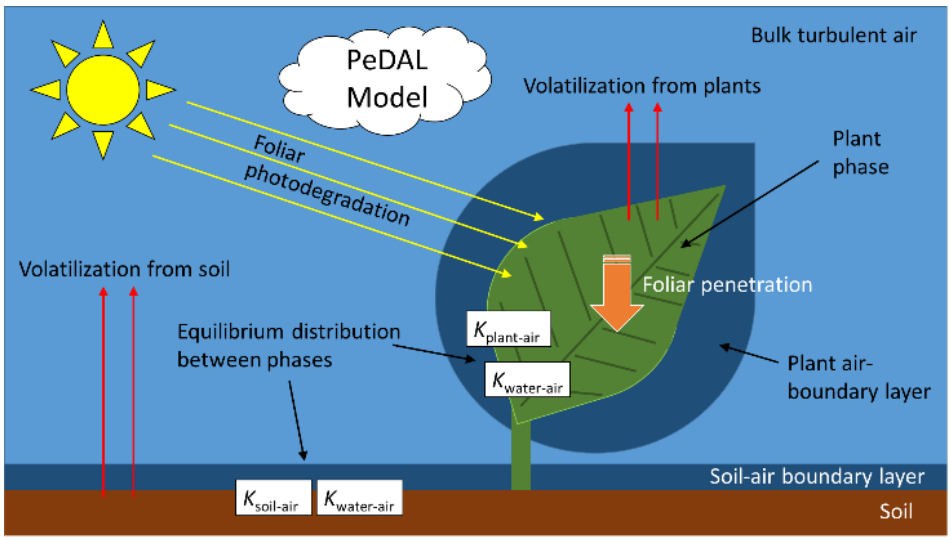

Figure 3. Conceptual Diagram of the PeDAL model.

field studies. We then used the reported field and meteorological conditions as input parameters in the PeDAL model and compared the modeled DT_{50} values to the measured ones. Next, we performed a sensitivity analysis on the photodegradation component of the model. Finally, we demonstrated how the PeDAL model could be used in practical situations by using it to predict how application timing (time of year and time of day) affects pesticide fate in a field and

to calculate emission fluxes for two separate applications, one with parathion and the other with chlorpyrifos, to potato crops in the Netherlands.

Methods

Model Overview

The PeDAL model uses the same standard agricultural field and processes that describe pesticide volatilization from plants and soils as the PLoVo model.[21,39] While the PLoVo model was designed specifically to explore the factors that affect pesticide volatilization from soil and plant surfaces, the PeDAL model incorporates additional processes, namely pesticide photodegradation from leaf surfaces and foliar penetration. The incorporation of these additional processes allows us to predict DT_{50} values, which indicate the rate at which pesticide concentrations decrease from leaves due to the combined effects of these processes. While leaf penetration does not remove the pesticide from the leaf, it is required to calculate DT_{50} since pesticide that has moved to the interior leaf layers is not available for volatilization or photodegradation.[40] Penetration may also decrease pesticide exposure to insects that crawl on leaf surfaces, but not to ones that chew or consume leaves. Wash-off of pesticides from leaf surfaces during precipitation is another process that decreases pesticide mass on leaf surfaces; however, we have not included this process in the current model because the extent of wash-off can vary considerably with the amount of precipitation, physicochemical properties of the active ingredient, effects of adjuvants in the formulation, and the timing of precipitation relative to the application.[41]

The standard agricultural field used in the PeDAL model is composed of soil, plant, and turbulent air compartments.[21] The soil compartment consists of soil, moisture in the soil, and a

soil-air boundary layer. The plant compartment contains plant material, plant-air boundary layer, and water on the plant surface. We set the volume of water on the plant surface at 25% relative to the volume of plant material; the method for selecting this default value was described in Taylor et al.[21] If the initial pesticide concentrations in the field compartments are known or can be calculated, the PeDAL model can be used to predict concentrations in the soil and plant compartments as a function of time after application. In many situations, however, it may be more useful to use the PeDAL model to predict the DT_{50} only since this output parameter is independent of initial concentrations due to the assumption that all processes affecting pesticide dissipation are first-order. The input parameters in the PeDAL model include ones that describe the pesticide physiochemical properties, the field and crop characteristics, and the meteorological conditions.

Specific Processes

Pesticide Volatilization from the Soil and Plant Compartments

The mass of pesticide that volatilizes from soil and plant compartments was calculated according to the multiphase partitioning approach.[21] We assume that volatilization from both compartments are independent of one another and the concentration in the turbulent air is always set to zero due to constant removal of pesticide by wind. Although the assumption is not ideal, the effects of this assumption on results are negligible.[21] The mass of pesticide that is initially present in each compartment is determined by the foliar intercept fraction (%*I*), which represents the percentage of pesticide that lands on leaves and is estimated using the International Union of Pure and Applied technical report on the subject.[42]

Pesticide volatilization from soil compartment

The first step in calculating volatilization from soil was to determine the fraction of pesticide in the soil-air boundary layer which was calculated using equation 1.

$$F_{\text{air-boundary(soil)}} = \frac{1}{1+K_{\text{soil-air}}\left(\frac{V_{\text{soil}}}{V_{\text{air-boundary(soil)}}}\right)+K_{\text{water-air}}\left(\frac{V_{\text{water(soil)}}}{V_{\text{air-boundary(soil)}}}\right)} \quad (1)$$

where $F_{\text{air-boudary(soil)}}$ is the fraction of pesticide in the air-boundary layer above the soil, $K_{\text{soil-air}}$ and $K_{\text{water-air}}$ are the soil-air and water-air partition coefficients, respectively, and V_{soil}, V_{water}, and $V_{\text{air-boundary(soil)}}$ are the volume of the soil compartment, volume of water in the soil compartment, and volume of the air-boundary layer above the soil compartment, respectively. Equation 2 is based off of 943 $K_{\text{soil-air}}$ measurements that included 22 pesticides, two types of soil, and a range of environmentally relevant temperatures and relative humidities used to calculate the $K_{\text{soil-air}}$ from the log $K_{\text{octanol-air}}$, relative humidity (RH), air temperature (T), and fraction organic carbon (f_{oc}) in the soil.[43]

$$\log K_{\text{soil-air}} = -26.2 + 0.714 \log K_{\text{octanol-air}} + 8291\frac{1}{T} - 0.0128 \cdot RH + 0.121 \log f_{\text{oc}} \quad (2)$$

Then, the mass of pesticide loss from the soil-air boundary layer to the turbulent air every hour was calculated using Fick's Law of Diffusion (equation 3).[44]

$$J_{\text{soil}} = -D_{\text{air}} \cdot \frac{c_{\text{air(turbulent)}} - c_{\text{air-boundary(soil)}}}{d_{\text{air-boundary(soil)}}} \quad (3)$$

where J_{soil} is the mass of pesticide lost from the soil-air boundary layer to the turbulent air per hour, $d_{\text{air-boundary(soil)}}$ is the depth of the boundary layer above the soil (which was fixed at 1 mm) and $c_{\text{air(turbulent)}}$ and $c_{\text{air-boundary(soil)}}$ are the concentrations in the turbulent air and in the soil-air boundary layer, respectively. D_{air} is the air diffusion constant and was determined using equation 4.[24]

$$D_{\text{air(T)}} = D_{\text{air(T,ref)}}\left(\frac{T}{T_{\text{ref}}}\right)^{1.75} \quad (4)$$

where $D_{air(T)}$ and $D_{air(T,ref)}$ are the air diffusion constants at the temperature of interest (T) and the reference temperature (T_{ref}).

Pesticide Volatilization from Plant Compartment

Pesticide volatilization from the plant compartment was calculated in a similar manner to the soil compartment. First, the fraction of pesticide in the boundary layer was calculated using equation 5.

$$F_{\text{air-boundary(plant)}} = \frac{1}{1+K_{\text{plant-air}}\left(\frac{V_{\text{plant}}}{V_{\text{air-boundary(plant)}}}\right)+K_{\text{water-air}}\left(\frac{V_{\text{water(plant)}}}{V_{\text{air-boundary(plant)}}}\right)} \quad (5)$$

where $F_{air\text{-}boundary(plant)}$ is the fraction of pesticide in the boundary layer surrounding leaves, $K_{plant\text{-}air}$ is the plant-air partition coefficient, and V_{plant} of plant material. $V_{water(plant)}$ is the volume of water present on the surface of leaves and is calculated according to equation 6.

$$V_{\text{water(plant)}} = \text{PWP} \cdot V_{\text{plant}} \quad (6)$$

where PWP is the plant water percentage relative to the volume of plant material. PWP was set at 25% based on the results obtained by Taylor et al.[21]

$V_{air\text{-}boundary(plant)}$ is the volume of the boundary layer surrounding the leaves of the plant and was calculated using equations 7 and 8.[45]

$$V_{\text{air-boundary(plant)}} = 2 \cdot \text{LAI} \cdot A_{\text{field}} \cdot d_{\text{air-boundary(plant)}} \quad (7)$$

$$d_{\text{air-boundary(plant)}} = 0.004\sqrt{\frac{l_{\text{leaf}}}{\text{WS}}} \quad (8)$$

where LAI is the leaf area index, A_{field} is the area of the field, $d_{air\text{-}boundary(plant)}$ is the thickness of the boundary layer surrounding the leaves, l_{leaf} is the leaf length, and WS is the wind speed.

Taylor et al. obtained a series of $K_{\text{plant-air}}$ predictive equations from the literature.[21] These equations were based on measurements for polychlorinated biphenyls (PCBs), hexachlorohexanes (HCHs), and polycyclic aromatic hydrocarbons (PAHs) so they may not be ideal for predicting the environmental behavior of pesticides due to the presence of polar functional groups on many pesticides that are absent on PCBs, HCHs, and PAHs. However, these equations were used because pesticide specific predictive plant-air equations are not currently available in the literature.

Equation 9, which was used previously by Komp and MacLachlan, was then used to correct $K_{\text{plant-air}}$ values so it was applicable to the observed temperature.[46]

$$K_{\text{plant-air(T)}} = K_{\text{plant-air(T,ref)}} \cdot e^{\left[\frac{\Delta H_{\text{i,plant-air}}}{R} \cdot \left(\frac{1}{T} - \frac{1}{T_{\text{ref}}}\right)\right]} \tag{9}$$

where $K_{\text{plant-air(T)}}$ and $K_{\text{plant-air(T,ref)}}$ are the plant-air partition coefficients at the temperature of interest (T) and the reference temperature (T_{ref}), respectively, $\Delta H_{\text{i,plant-air}}$ is the enthalpy change associated with chemical *i* transfer from the plant phase to the air, and R is the gas constant.

Second, the mass of pesticide loss from the plant-air boundary layer to the turbulent air every hour was calculated using Fick's Law of Diffusion (equation 10).[44]

$$J_{\text{plant}} = -D_{\text{air}} \frac{c_{\text{air(turbulent)}} - c_{\text{air-boundary(plant)}}}{d_{\text{air-boundary(plant)}}} \tag{10}$$

where J_{plant} is the hourly mass of pesticide lost from the plant-air boundary layer to the turbulent air and $c_{\text{air-boundary(plant)}}$ is the concentration of pesticide in the plant-air boundary layer.

A predicted emission flux value from both compartments was calculated for each one-hour time step (equation 11).

$$J_{\text{i,total}} = \frac{J_{\text{i,plant}} + J_{\text{i,soil}}}{A_{\text{field}}} \tag{11}$$

where A_{field} is the area of the field and $J_{i,total}$ represents the combined emission flux from the soil and plant compartments. The soil compartment will be largely ignored here except when demonstrating the model's ability to predict an emission flux following pesticide application.

Pesticide Photodegradation

To incorporate photodegradation into our model, we first compiled available pesticide photodegradation rates from the literature[29,47–50] that met the following criteria. First, all photodegradation rates we included were measured on the surface of a leaf or leaf proxies, such as paraffin wax or extracted leaf wax. We did not use pesticide photodegradation rates measured in solution or on other surfaces (such as glass, fruit wax, and soil) since these rates are not expected to accurately represent those on leaf surfaces.[51] We also did not consider photodegradation of pesticide present inside water droplets on the plant surface since no data is available about this process. Second, only photodegradation rates that were determined in laboratory experiments were included. We used this criterion since laboratory experiments, when compared to experiments in the field, result in more accurate photodegradation rates and apply to specific radiation levels, specific application concentrations, and control for losses from another process, such as volatilization. Third, all rates were measured with solar simulators set to produce light that closely matches the spectrum produced by the sun and received at Earth's surface. This means that results from experiments using wavelengths below ~280-300 nm (*i.e.* in the ultraviolet C range) were not used. We found photodegradation rates that met these criteria for fifteen pesticides; however, the field dissipation rate had also been measured for only the following six pesticides, which were included in our model evaluation exercise: 2,4-dichlorophenoxyacetic acid (2,4-D), azadirachtin, chlorothalonil, chlorpyrifos, fenitrothion, and parathion (Table A1). In all cases, the photodegradation rates we used were obtained with experiments conducted at a constant radiation intensity and using the active ingredients (without adjuvants) rather than a commercial formulation.

To incorporate the effects of radiation intensity on pesticide photodegradation in the PeDAL model, we linked it to Bird's Clear Sky Model[30,52] (BCSM). BCSM is a broadband algorithm based on a series of algebraic expressions with various inputs (Table A2) that can be altered by the user to provide estimates for the hourly clear sky solar radiation for any location. The solar radiation estimations provided by BCSM were then adjusted by a cloud coverage factor. This factor was developed based on the work of Matuszko in Krakow, Poland.[53] Matuskzo measured the intensity of sunlight on the Earth's surface as it changed with the height of the sun above the horizon and degree of cloudiness. Cloudiness was measured in terms of octas with one octa representing one-eighth of the sky covered. Matuskzo's data were then normalized with respect to the intensities for zero octas. This was done so that zero octas could serve as a baseline and then the rest of the data could be used to develop an equation to represent how clouds increase or decrease the intensity of solar radiation at the Earth's surface. This was especially useful since it allows for the easy alteration of the estimation made by BCSM, which applies to a scenario when no clouds are in the sky. We used equation 12 to correct for cloud coverage.

$$I_{\mathrm{act}} = (-0.0008 \cdot \mathrm{CC}^4 + 0.0121 \cdot \mathrm{CC}^3 - 0.0629 \cdot \mathrm{CC}^2 + 0.0666 \cdot \mathrm{CC} + 1.0026) \cdot I_{\mathrm{BCSM}} \qquad (12)$$

where I_{act} and I_{BCSM} are the actual solar radiation intensity (used in the PeDAL model) and the solar radiation intensity predicted by BCSM, respectively, and CC is the cloud coverage in octas. Percent cloud coverage is coverted to that in octas by dividing the percent value by 12.5. Equation 12 results in a minimal change to I_{act} compared to I_{BCSM} for cloud coverage values <20% and a decrease to ~40% of the I_{BCSM} when there is 100% cloud coverage. The data used to produce equation 12 was collected in Krakow, Poland and may not be perfectly suitable for all locations and the type of clouds may also play a role in the amount of radiation reaching plants on the Earth's surface We used the hourly radiation intensities to calculate hourly photodegradation rates with equation 13, which is based on that used by Wolters et al.[27]

$$k_{\text{photo(act)}} = \frac{k_{\text{photo(ref)}}}{I_{\text{ref}}} \times 0.75 I_{\text{act}} \quad (13)$$

where $k_{\text{photo(ref)}}$ and I_{ref} were the reference photodegradation rates and associated light intensities obtained from the literature studies (Table A1), $k_{\text{photo(act)}}$ is the actual photodegradation rate after adjustment for the light conditions in the field, and I_{act} is the actual solar radiation intensity obtained either from BCSM (equation 12) or from field measurements. The factor of 0.75 was used in equation 13 to account for the angle of the light hitting the surface of the leaves. This factor was needed because in laboratory photodegradation experiments, the radiation is perpendicular to the leaf surfaces whereas in the field, this angle varies due to the changing position of the sun and movement of leaves with the wind. We trialed several values ≤1 and found that 0.75 provided the best fit between modeled and measured DT_{50} values; however, the optimal value could vary with crop species, depending on orientation of the crop's leaves.

The mass of pesticide 'i' lost from leaf surfaces due to photodegradation ($m_{\text{i,photo}}$) was calculated for each one-hour time step using equation 14:

$$m_{\text{i,photo}} = m_{\text{i,plant(av)}} \times \left(1 - e^{-k_{\text{i,photo(act)}}}\right) \quad (14)$$

where $m_{\text{i,plant(av)}}$ is the mass of pesticide 'i' in the plant compartment that is available to undergo photodegradation (*i.e.* the mass on the leaf surface only, not including that in the leaf interior).

Pesticide Penetration into Leaves

Foliar penetration of pesticides is dictated by the properties of the pesticide active ingredient and formulation components, weather conditions, and characteristics of the leaf.[25] Due to the limited available data regarding penetration rates (k_{pen}), we used a generic value of 0.002 h^{-1}, which we selected from the range of values discussed by Houbraken et al.[23] Penetration differs from the other processes included in the PeDAL model because it is not considered a loss process.

Whereas volatilization removes pesticide from the system and photodegradation transforms it into another chemical, penetration simply reduces the amount of pesticide available on the leaf surface. Once the pesticide penetrated into the leaf, we considered it unavailable for volatilization or photodegradation.[40] The mass of pesticide "i" undergoing penetration into the leaf during a one-hour time step ($m_{\mathrm{i,pen}}$) was calculated with equation 15:

$$m_{\mathrm{i,pen}} = m_{\mathrm{i,plant(av)}} \times \left(1 - e^{-k_{\mathrm{i,pen}}}\right) \tag{15}$$

Model Evaluation

We evaluated the PeDAL model by comparing modeled and measured DT_{50} values. This was accomplished by first compiling a list of 49 DT_{50} values measured during field studies; these values were obtained from 36 publications. We also compiled the parameters describing the crop, field, and meteorological data for these studies (Tables A3-5). We only considered DT_{50} values for the six pesticide active ingredients for which we found *both* photodegradation rates (Table A1) and DT_{50} values in field studies. The DT_{50} values we obtained were measured on 25 different plant surfaces, experiments were conducted during a wide range of weather conditions from locations at latitudes ranging from 52.5°N to 45.6°S, and applications took place in eight different months. The criteria we used to select the data for model evaluation, and the approach we used to determine measured DT_{50} values, are included in the Appendix (Section A1).

In this exercise, we did not consider photodegradation or volatilization from the soil compartment because details about the soil compartment were not included in most of the literature sources that reported DT_{50} values. Thus, we set the foliar intercept fraction to 100% in all cases. All other input values, and references to support their selection, are included in Tables A3-5.

We used a constant temperature (T_{input}) to calculate plant-air partition coefficients (equation 16).

$$T_{\text{input}} = \frac{T_{\text{avg}} + T_{\text{max}}}{2} \tag{16}$$

where T_{avg} was the average temperature reported and T_{max} was the maximum temperature reported for the field experiment. T_{input} was used because the literature reports didn't include detailed hourly weather data and since volatilization increases exponentially with temperature, T_{avg} would have likely underestimated volatilization.[46]

The plant-air partition coefficient equation used in all simulations was the equation determined by Komp and McLachlan for clover (equation 17).[54] We used the clover equation because plant-air partition coefficients for the actual plants used in the field experiments aren't available in the literature.

$$K_{\text{plant-air}} = 10^{(0.7 \log K_{\text{octanol-air}} + 0.15)} \tag{17}$$

To determine the effect of adding foliar photodegradation and penetration to our model, scenarios used in the evaluation were modeled using a variety of process combinations (e.g. volatilization and photodegradation, volatilization and penetration, volatilization only, photodegradation with penetration, and photodegradation only).

Sensitivity Analysis

To determine the effects of photodegradation on DT_{50} values for pesticides with a wide range of physicochemical properties, DT_{50} values were modeled for over 3000 hypothetical chemicals using three rates for pesticide photodegradation on leaf surfaces. Sensitivity analysis for other aspects of the model, i.e. ones not concerning photodegradation, have been conducted

previously.[16,17] To represent fast photodegradation, the rate for 2,4-D[47] was used (2.90×10^{-2} h^{-1} @ 320 W m^{-2}) while the rates for parathion[50] (2.22×10^{-2} h^{-1} @ 500 W m^{-2}) and chlorpyrifos[29] (1.37×10^{-3} h^{-1} @ 1000 W m^{-2}) were used to represent moderate and slow photodegradation, respectively. The results were displayed on chemical space diagrams depicting the log $K_{plant\text{-}air}$ against the log $K_{water\text{-}air}$, with the magnitude of the cumulative percent loss in 24 h (CPL_{24h}) displayed using contoured background shading. All input parameters used in this exercise are provided in Table A6.

In addition, we investigated the effects of photodegradation on DT_{50} by modeling the behavior of a selected pesticide (the insecticide parathion) applied to a clover using default conditions (Table A7) and various light intensity regimes based on the chosen sites' latitudes and elevations. Modeled concentrations were obtained for diurnal light regimes representing those during the Spring Equinox and Summer Solstice for two extremes; one on the equator (Quito, Ecuador) and the other at a high latitude (Fairbanks, AK, USA). In addition to those extremes, three sites within the continental United States were chosen: Orlando, FL; Logan, UT; Duluth, MN. We compared the modeled DT_{50} values generated under these situations to that obtained when a constant photodegradation rate of 0.0222 h^{-1} (*i.e.* the rate obtained with continuous irradiation at 500 W m^{-2}) was used since this simpler approach is often used in pesticide fate models. Parathion was selected because its photodegradation rate falls in the middle of the range found for pesticides used in the model evaluation. Volatilization was excluded in this exercise so that the photodegradation component of the PeDAL model could be examined alone. We defined the 'photodegradation DT_{50}' as the amount of time needed for the pesticide concentration to decrease to half of the original concentration when losses were due to photodegradation alone.

Using PeDAL to Explore Aspects of Pesticide Dissipation

We investigated how application timing, both in terms of season and time of day, affects pesticide dissipation. This was accomplished by first modeling a spring and summer application in Logan, Utah, USA, for the six pesticides used in model evaluation. Second, we modelled pesticide concentrations when the application occurred a 6am, noon, and 6pm for the same spring and summer conditions. Input parameters for the investigation of application timing are included in Table A8.

We also used the PeDAL model to estimate pesticide emission fluxes from sprayed fields. We used input data designed to replicate the weather and crop conditions during two field studies described in the literature. In these studies, parathion[55] and chlorpyrifos[40] were applied to potato fields in The Netherlands. We defined our emission flux as the mass of pesticide loss per time from the system due to volatilization; we included volatilization from both the soil and plant compartments since volatilization has been shown to be slower from soil than from plants.[56,57] $\%I$ was estimated using the value for potatoes reported in the International Union of Pure and Applied Chemistry's (IUPAC) technical report.[42] Input parameters for the prediction of emission flux for these scenarios, including field and meteorological conditions, are provided in Table A9.

Results and Discussion

Model Evaluation

Measured DT_{50} values from the literature are compared to modeled values generated for the same environmental and field conditions in Figure 4. The descriptive parameters (slope of 0.92,

y-intercept of 0.06, R^2 of 0.76, and root mean square error (RMSE) of 0.94 days) indicate overall robust model design and effectiveness at predicting pesticide dissipation rates. The full list of pesticide-plant combinations, along with measured and modeled DT_{50} values for each of the 49 cases is available in Table A10. Considering that the modeled DT_{50} values are strongly affected by the input values used, we hypothesize that an even better match between modeled and measured results would have occurred if more specific data related to the actual meteorological conditions and plant characteristics had been available in the literature sources from which we obtained the measured DT_{50} values. In addition, the available photodegradation rates (Table A1) were not necessarily measured on the same plant species as the measured DT_{50} values. For example, the available photodegradation rate for chlorpyrifos was measured on soft shield fern (*Polystichum setiferum*)[29] (Table A1) whereas the associated DT_{50} values were measured on the leaves of several other plants (Chinese cabbage, collards, cotton, kale, orange, potato, purple tansy, and rose) (Table A10). Information about the degree to which pesticide foliar photodegradation rates vary among plant species is limited; however, a previous report indicated that the photodegradation half-life of the insecticide fenthion varied by nearly a factor of five depending on the type of fruit wax to which

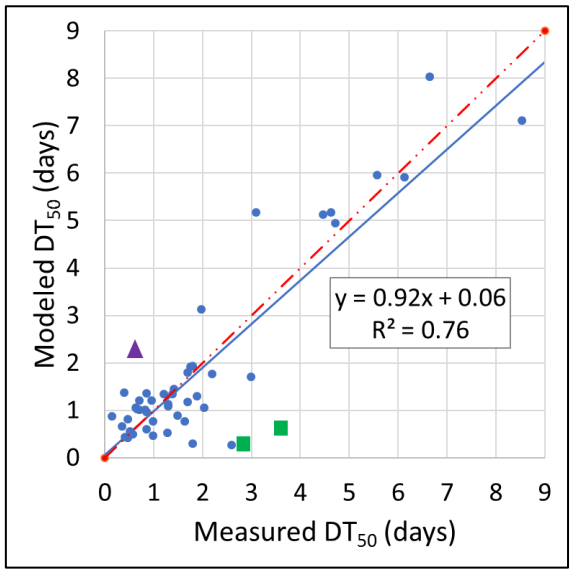

Figure 4. Measured versus Modeled DT_{50} Values. The solid line represents the trend line for modeled versus measured DT_{50} values(n=49, RMSE=0.94 days). The dashed line represents the 1:1 line. The green squares represent DT_{50} values from two studies with chlorothalonil and the purple triangle represents the DT_{50} value for the study with chlorpyrifos on purple tansy.

it was applied.[58] This suggests that photodegradation rates used for modeling purposes should be determined on the pesticide-crop surface combination that is being modeled whenever possible.

Another likely source of error in the modeled DT_{50} values in Figure 4 is our use of the $K_{\text{plant-air}}$ predictive equation developed for clover even though other plants were used in the field experiments. While there is evidence that plant-air partitioning varies among plant species,[46,54,59] we used the clover equation since equations for the plants actually used in the field studies are not available. Another limitation is that the $K_{\text{plant-air}}$ values and photodegradation rates we used in the model were measured for pure active ingredients rather than formulations. The adjuvants in formulations can effect pesticide volatilization rates from soils, glass, and other surfaces[60–63] and formulated epoxiconazole has been shown to penetrate into the leaf tissue more readily than pure epoxiconazole.[31] However, the potential effects of formulation adjuvants on pesticide volatilization from leaf surfaces are extremely limited in the literature.[31] Differences in photodegradation kinetics for pure versus formulated active ingredients have been reported in a few cases, with the formulation photodegrading significantly quicker in some cases.[64–66]

An interesting observation is that the modeled DT_{50} values for the fungicide chlorothalonil were much lower than the measured ones obtained following application to peanuts[67] and Chinese cabbage[68] (green squares in Figure 4), and that these correlations were notably worse than those for the other five pesticides investigated in the evaluation. We found that removing the two data points for chlorothalonil improved the slope of the fitted line (from 0.92 to 0.96), the correlation coefficient (from 0.76 to 0.83), and the RMSE (from 0.94 to 0.79 days). The fitted line without these points was $y=0.96x + 0.09$. This may indicate that better input parameters for describing chlorothalonil's behavior on foliage are needed.

A second notable observation is that the modeled DT_{50} for the insecticide chlorpyrifos applied to purple tansy[69] was considerably higher than the measured one (purple triangle in Figure 4). In this experiment, the application took place when winds were calm, but the wind speed

increased dramatically soon after application such that the average wind speed was 5.9 m/s during the 6-h period following application and averaged 8.2 m/s during the 4th hour after application. We hypothesize that the large discrepancy between modeled and measured DT_{50} values in this case mainly resulted from fast volatilization of 'just-applied' pesticide in windy conditions. Previous studies have reported that the binding strength between pesticides and leaf surfaces increases during the hours immediately after application.[41]

Finally, Table 1 and Figure A1 show how the DT_{50} correlation parameters varied when we incorporated different combinations of processes in the model. Most importantly, we found that the full PeDAL model produced the best overall results, highlighting the value of including as many dissipation processes as possible. Nonetheless, the correlation was nearly as good when only volatilization and photodegradation were included, with the additional inclusion of foliar penetration improving the correlation only to a small degree. All process combinations that did not include *both* volatilization and photodegradation resulted in poor correlation, also demonstrating that these two processes should be prioritized in modeling efforts.

Table 1. Descriptive Parameters for Measured versus Modeled DT_{50} Values when Various Combinations of Processes were used in the PeDAL Model. Correlation plots are provided in Figure A1. CI indicates confidence interval.

Processes	**Equation**	**R^2**	**RMSE (days)**	**95% CI for slope**	**95% CI for y-intercept**
All (full PeDAL model)	y = 0.92x + 0.06	0.76	0.95	±0.15	±0.40
Volatilization & Photodegradation	y = 0.74x + 0.22	0.74	0.97	±0.11	±0.42
Volatilization & Penetration	y = 1.45x + 1.33	0.30	4.69	±0.64	±1.73
Volatilization only (PLoVo model)	y = 1.37x + 1.23	0.28	4.50	±0.64	±1.72
Photodegradation & Penetration	y = 0.79x + 6.40	0.09	7.48	±0.73	±1.94
Photodegradation only	y = 0.72 x + 5.54	0.08	6.65	±0.7	±1.89

Sensitivity Analysis

The influence of the photodegradation rate on the CPL_{24h} for chemicals with a wide range of partitioning properties is illustrated in the chemical space diagrams in Figure 5. The size of the red area shows the degree to which the dissipation rate changes as the photodegradation rate increases for chemicals with different properties. Plots like these could help drive the direction of future research on pesticide photodegradation. For example, chemicals that fall near the bottom left of these diagrams (*i.e.* those with relatively low $K_{plant\text{-}air}$ and $K_{water\text{-}air}$ values) tend to volatilize rapidly under most conditions; thus, measuring precise photodegradation rates for them is less important. Instead, research attention should be directed towards measuring the photostability of chemicals whose fate is most sensitive to photodegradation rates, such as those that fall in the area that is dark blue in Figure 5a, but red/yellow in Figure 5c. Figure 5c also shows that it is less important to measure precise partition coefficients for chemicals that photodegrade quickly. Understanding how CPL_{24h} is affected by various parameters and field conditions is an important

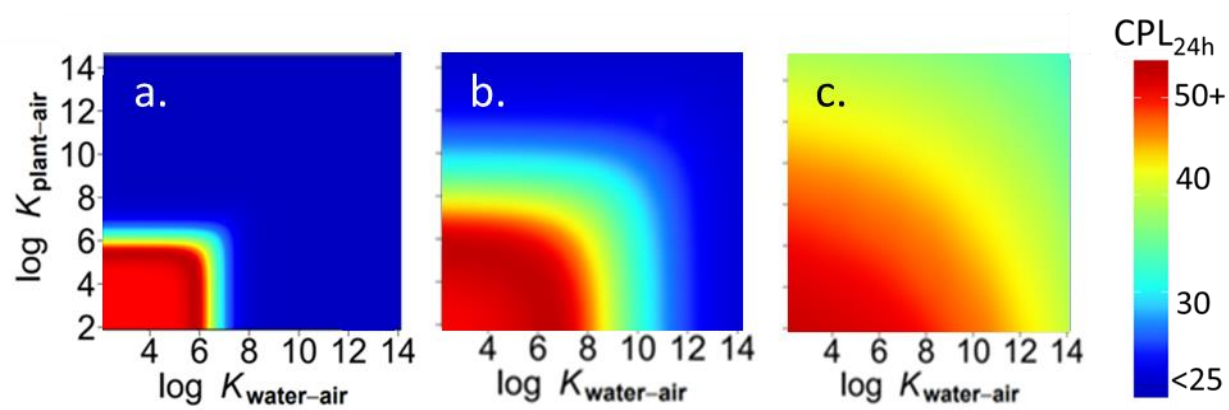

Figure 5. Chemical Space Diagrams showing CPL_{24h} values (%) for an Application to a Generic Plant under Default Conditions with Three Levels of Photodegradation. (a) slow photodegradation ($k_{photo(ref)}$=1.37x10^{-3} h^{-1} and I_{ref}=1000 W m^{-2}); (b) moderate photodegradation ($k_{photo(ref)}$=2.22x10^{-2} h^{-1} and I_{ref}=500 W m^{-2}); and (c) fast photodegradation ($k_{photo(ref)}$=2.90x10^{-2} h^{-1} and I_{ref}=320 W m^{-2}).

component of precision agriculture development since rapid pesticide dissipation may mean minimal crop protection whereas persistence at low concentrations may result in increased development of pest resistance to pesticides. It is important to note that the shading positions in Figure 5 change when the meteorological conditions and crop details change; for example, such variations are illustrated in Figure A2 (using input parameters from Table A6).

An example scenario demonstrating photodegradation DT_{50} sensitivity to location and time of year is shown in Figure 6. In this scenario, modeled DT_{50} values for the insecticide parathion are shown for the situation in which volatilization is excluded, all other default values (Table A7) are used, and the light conditions (with diurnal variations) represent those at five example locations on the Northern Hemisphere Spring Equinox (*i.e.* in March) and Summer Solstice (*i.e.* in June). In the constant photodegradation example, we used a solar radiation intensity of 500 W m^{-2} since this

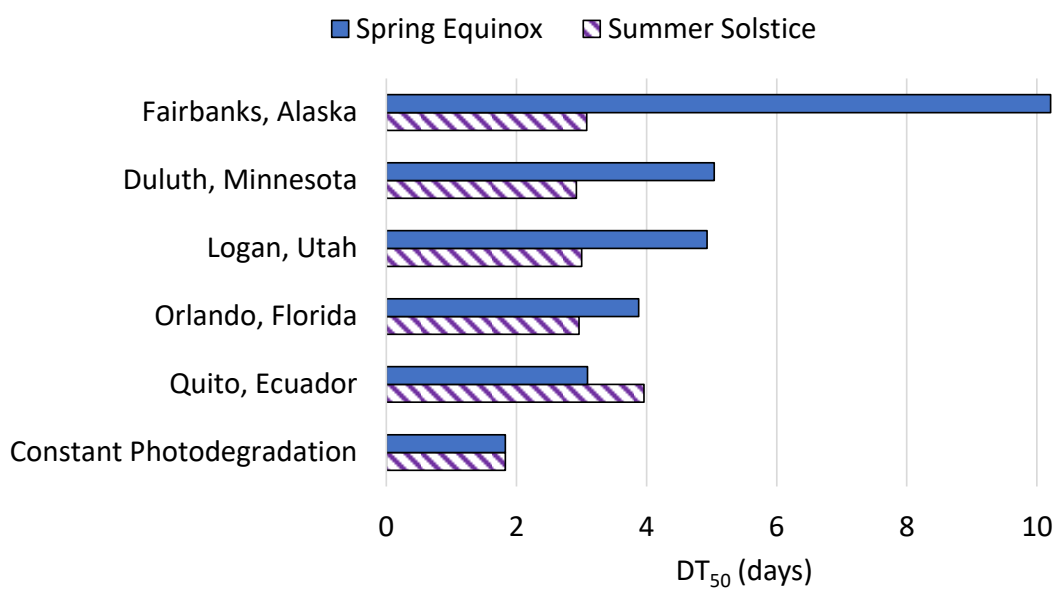

Figure 6. Photodegradation Sensitivity Analysis for Parathion using Default Input Parameters and the Light Intensity Conditions, with Diurnal Variation, at Five Locations during Two Seasons, as well as with a Constant Irradiation of 500 W m^{-2}. Volatilization was excluded here so all pesticide dissipation is due to photodegradation.

is the generic reference intensity used in some pesticide fate models;[25,27,34] this intensity resulted in a constant photodegradation rate of 0.0222 h^{-1}.[50] The differences between spring and summer photodegradation DT_{50} values increased with distance from the equator, with differences of 0.8 and 2.1 days being observed for Quito, Ecuador (latitude 0.18 ºS) and Duluth, MN (latitude 46.79 ºN), respectively. A dramatic difference in modeled DT_{50} values was observed for Fairbanks, Alaska (latitude 64.84ºN), where the DT_{50} varied from 10.2 to 3.1 days between seasons. The constant irradiation example demonstrates the degree to which use of a generic photodegradation rate constant could lead to inaccurate predictions for DT_{50}. Altogether, these results demonstrate that pesticide fate models should ideally include modules for estimating photodegradation rates that are specific to the light intensity conditions representing those for the timing and location of interest.

Using PeDAL to Explore Aspects of Pesticide Dissipation

Question 1: How is DT_{50} affected by the season of application?

Figure 7 shows how the PeDAL model can be used to investigate practical questions, such as how the season of application could affect DT_{50} values. For each of the investigated pesticides, dissipation was clearly more rapid during summer than spring and this was due to a combination of higher summer temperatures leading to increased volatilization and longer, more intense summer light regimes leading to increased photodegradation. The relative contributions of each process are provided in Figure A3 for the insecticide parathion. Among the six investigated pesticides, the difference in DT_{50} between seasons was most dramatic for chlorpyrifos (Figure 7) due to it being the most photostable and due to the lower temperatures in spring resulting in very little volatilization. The other five pesticides had modeled DT_{50} values of <5 days for both sets of conditions, with much shorter DT_{50} values in the summer. These results show, for example, how

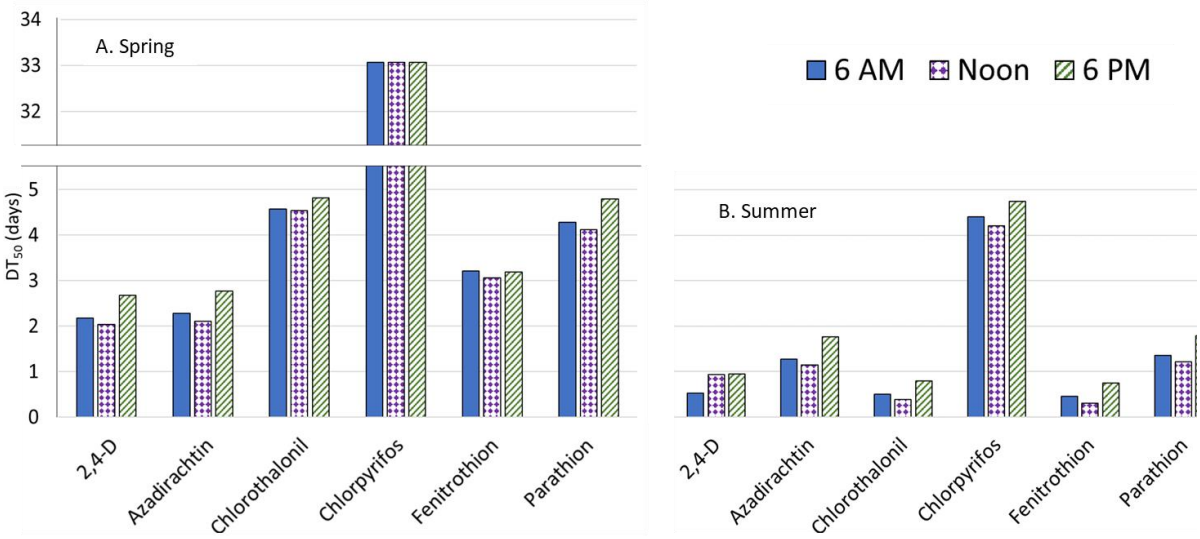

Figure 7. Comparison of Modeled DT_{50} Values of Selected Pesticides at Different Application Times when Applied to Clover under Typical Conditions in Logan, Utah, USA in Spring and Summer. Input parameters for these scenarios are found in Table A8. (A) Spring and (B) Summer.

the PeDAL model could be used to calculate condition-specific Reentry Intervals for field workers and Pre-Harvest Intervals for food crops.

Question 2: How is DT_{50} affected by application time of day?

Figure 7 also shows how the time of application affects modeled DT_{50} values for the six investigated pesticides. The time of day had less of an affect than season of application; however, the DT_{50} values were always the lowest for noon applications and longest for 6pm applications. For example, the DT_{50} values for 2,4-D, azadirachtin, and parathion were 16 hours longer when applied at 6pm compared to noon in the spring. This occurred because pesticides applied at 6pm encountered lower temperatures and less time with intense sunlight than did those applied at noon. Under summer conditions, the predicted DT_{50} values for 2,4-D, fenitrothion, and azadirachtin were 1, 11, and 15 hours longer when applied at 6pm compared to noon. These results show that the application timing could have significant effects on pesticide efficacy and demonstrates how the PeDAL model could be employed in refining pesticide application strategies. For example, the

longer persistence of pesticides applied in the evening could result in increased efficacy against pests that are active at night and therefore lead to an overall reduced quantity of pesticide applied.

Question 3: Can the PeDAL model accurately estimate pesticide emission flux?

Two initial fluxes were reported by van den Berg et al. for parathion emission from a potato field: 1.40 mg m^{-2} h^{-1} when calculated using the aerodynamic method and 2.62 mg m^{-2} h^{-1} when using the Bowen ration method.[55] When we used input parameters in the PeDAL model designed to replicate van den Berg's field experiment (Table A9), we obtained a modeled emission flux of 1.69 mg m^{-2} h^{-1}, which is remarkably similar to the average of the measured values. Leistra et al. conducted a similar field experiment and reported chlorpyrifos emission rates from a potato field using four different methods: the aerodynamic method, energy balance method, relaxed eddy accumulation method, and the plume dispersion method.[40] Depending on the method used, the initial emission flux varied between 2.74 and 6.72 mg m^{-2} h^{-1}. When using input parameters designed to replicate this field experiment (Table A9), we obtained a modeled flux of 1.16 mg m^{-2} h^{-1}. In this case, the modeled flux was lower than the range of measured fluxes but within the same order of magnitude. Although more experiments should be conducted to evaluate the model's ability to predict an emission flux, these results show that the PeDAL model could become a useful tool for estimating pesticide-specific, condition-specific emission fluxes for use in atmospheric dispersion and transport models that predict pesticide concentrations in air in the vicinity of agricultural fields. The advantage of the PeDAL-model approach is that it is significantly faster, easier, and cheaper than other methods typically used to estimate pesticide fluxes from agricultural fields.

Conclusion

The work presented here shows that the PeDAL model is capable of simulating pesticide dissipation following application to a planted field with the newly developed photodegradation component that is specific to the chemical and conditions being modeled. A limitation is that it is currently designed to estimate pesticide dissipation for pesticide that lands on the outer canopy of plants; with additional field work, additional complex processes such as pesticide behavior in deeper portions of foliage that receive less sunlight and wind, could be included. Additional laboratory foliar photodegradation experiments would allow for expanded use by providing more pesticide photodegradation rates on leaves. Future studies should include experiments to determine $K_{\text{plant-air}}$ values, foliar photodegradation rates, and penetration rates into leaves that are specific to the pesticide-plant combination that is being modeled in order for these inputs to be as accurate as possible. Ideally, these studies would also examine the influence of adjuvants so that any formulation effects can be accounted for in the PeDAL model. Similarly, extensive studies focused on the influence of precipitation on pesticide wash-off would make the model more widely applicable. Without the inclusion of a wash-off component, the PeDAL model should only be used for scenarios without rainfall or scenarios when rainfall does not occur for several days following application.

CHAPTER 3: PESTICIDE FOLIAR PHOTODEGRADATION EXPERIMENTS

Introduction

Pesticide usage enables growers to produce larger and higher-quality crop yields that can be used to feed larger numbers of people which results in economic benefits for growers and consumers. Estimates suggest that the use of pesticides prevents the U.S. agricultural industry from losing tens of billions of dollars per year due to crop losses caused by pests.[5] It is unsurprising, therefore, that the Food and Agricultural Organization of the United Nations has estimated that global use of pesticides for agricultural use totaled nearly 6 billion kilograms in 2018.[70] However, this large use becomes problematic when considering the negative effects that pesticides can have on humans, other organisms, and the environment when reaching non-target areas. Pesticides have been linked to a variety of diseases in humans and contamination of surface and ground water, soil, and vegetation has the potential for further harm to any organisms that come in contact with those contaminated areas.[3]

To continue to reap the benefits of pesticides while minimizing their potential for harm, environmental fate models that accurately simulate pesticide behavior following application must be developed and utilized. Ideally, these types of models will promote decreased, but more effective usage of pesticides that maintains the benefits of crop protections while minimizing the associated risk. One such model is the Pesticide Dissipation from Agricultural Land (PeDAL) model.[32] Using relevant meteorological inputs, the chemical properties of the pesticide, and the physical properties of the plants and soils to which the pesticide is applied, the PeDAL model simulates the environmental fate of pesticides following their application. Multiphase partitioning and Fick's Law of Diffusion are used to predict volatilization. Foliar photodegradation is calculated

in the model using chemical-specific photodegradation rates from the literature which are modified based on the intensity of sunlight predicted in the field (sunlight intensity is estimated in the PeDAL model by linking it with Bird's Clear Sky Model[30]). The PeDAL model also includes a generic foliar penetration component. While the volatilization component of the model has been previously evaluated[21], the photodegradation component is a limiting factor in the expanded use of the model. Despite the importance of foliar photodegradation to the chemical fate of applied pesticides, there are few measurements of these photodegradation rates for pesticides. The need for using pesticide-specific foliar photodegradation rates in predicting chemical fate is exemplified by the large difference in the photoreactivity of select pesticides; chlorpyrifos[29] has a rate of 1.37×10^{-3} h^{-1} at 1000 W m^{-2} while cycloxydim[28] has a rate of 0.11 h^{-1} at 400 W m^{-2} while on leaf surfaces. The majority of studies that have investigated foliar photodegradation are further limited by their use of extracted waxes instead of intact leaves. Of the 18 pesticide photodegradation rates on leaf surfaces reported in the literature, only one has been measured on intact leaves.[29] The other 17 have used extracted waxes from leaves or other wax types, such as paraffin wax, to simulate leaf surfaces. In addition to potential surface differences between these waxes and intact leaves, fenthion has been shown to have a photodegradation rate that can vary by a factor of up to 5 depending on the type of fruit wax it is irradiated on.[58] This suggests that photodegradation rates used in predicting pesticide behavior should be obtained on the same surface being modeled whenever possible, although initial PeDAL model validation indicated that this is likely not a large source of deviation between modeled pesticide dissipation and what is measured in the field.[32] Similarly, the presence of adjuvants in pesticide formulations could impact pesticide photodegradation. This influence has been examined in the past with varying degrees of difference in photoreactivity between the pesticide active ingredient and formulated product.

A series of experiments were conducted to obtain foliar photodegradation rates for pesticides commonly used on alfalfa (active ingredients: chlorpyrifos, lambda-cyhalothrin,

indoxacarb) on the surface of alfalfa leaves. Differences in photodegradation were examined for these chemicals as pure active ingredient dissolved in solvent and as part of commercial pesticide formulations like would be applied in agricultural fields. Finally, these new obtained rates were used as inputs in the PeDAL model to model conditions reported in published field dissipation/persistence studies for these chemicals. Finally, the use of these newly measured rates was demonstrated by modeling the conditions reported in the literature for two field dissipation/persistence studies.

Materials & Methods

Chemicals & Reagents

Standards of chlorpyrifos (98%, Millipore Sigma), lambda-cyhalothrin (99.5% purity, Fisher Scientific), indoxacarb (97.9%, LGC Dr. Ehrenstorfer), chlorpyrifos-d10 (>97.5%, Fisher Scientific), tertbuthylazine-d5 (99.5%, CDN Isotopes), p-nitroanisole (>98%, Fisher Scientific), and pyridine (99%, anhydrous, Fisher Scientific) were purchased from various manufacturers.

Commercial formulations containing the active ingredients chlorpyrifos, lambda-cyhalothrin, and indoxacarb were obtained from local agricultural stores. More information on the chosen pesticides is included in Table 2.

Table 2. Pesticide Active Ingredient and Formulation Information

Active Ingredient	Chlorpyrifos	Lambda-cyhalothrin	Indoxacarb
Formulation name	Drexel® Chlorpyrifos 4E-AG	Warrior II with Zeon Technology®	Steward® EC
Pesticide class	Insecticide	Insecticide	Insecticide
Active ingredient content % (w/w)	44.9%	22.8%	15.84%
Active ingredient structure	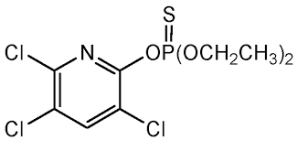	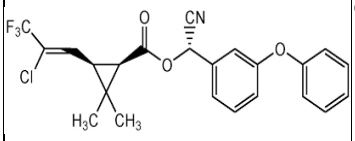	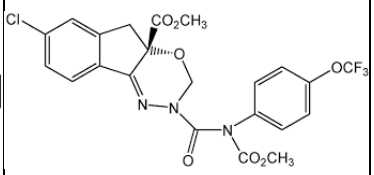
Other ingredients	No information available	Titanium dioxide, petroleum solvent, other (concentration unavailable)	Octanol (1-5%), alkyl sulfonate salt (5-10%), other (69.16-78.16%)

High-performance liquid chromatography (HPLC)-grade reagent alcohol (89-91% ethanol), and Optima-grade hexane, ethyl acetate and acetone were purchased from Fisher Scientific. HPLC-grade acetonitrile was purchased from Thermo Scientific. Purified water was produced using a Milli-Q water system.

Graphitized carbon black (ENVI-Carb Packing) was purchased from Sigma Aldrich and Florisil (60-100 mesh size) was purchased from Thermo Fisher.

Experimental Procedures

Leaves

Alfalfa (*Medicago sativa*) leaves were obtained from the Greenville Research Farm (Logan, Utah) on the same day that experiment was conducted. Experiments were performed in the August and September with fully grown alfalfa leaves. Individual leaves had their stems threaded through a slit that was cut into the polytetrafluoroethylene septa of gas chromatography (GC) vial caps which were then screwed onto GC vials that contained deionized water (Figure 8). This setup aided in preserving leaf condition for the length of the experiment and in positioning the samples prior to irradiation. During trial runs, leaves became dried and discolored without the presence of water. After the necessary number of samples were prepared, each GC vial was taped to the sample tray so that the alfalfa leaf was positioned parallel to the sample tray of an Atlas SunTest CPS+ solar simulator. This ensured that the leaves remained in a constant position for the duration of the experiment. In order to correct for any contamination of the leaves prior to collection, several leaves were collected and analyzed as field blanks.

Figure 8. Alfalfa Leaf Setup for Photodegradation Experiments. For real experiments the stem of the leaf was threaded through the cap further so that the leaf was in a more stable position.

Pesticide Application

A Hamilton syringe was then used to apply the appropriate mass of the chemical being studied. Application solutions were prepared by dissolving the pure active ingredient or commercial formulation in ethyl acetate. Typical field applications involve dissolving the formulation in water prior to application, however, ethyl acetate was used instead because it had the necessary solubility for the chosen pesticides but did not take as long to evaporate as water would have. Applications were made so that the initial application on each leaf was 2800 ng/cm^2, 336 ng/cm^2, and 1230 ng/cm^2 for chlorpyrifos, lambda-cyhalothrin, and indoxacarb, respectively. These values were chosen to represent concentrations that would be expected when making a field application according to the recommend application rates on the commercial formulation labels (Table 3).

Table 3. Application Rates Based on Recommendations of Commercial Formulations

Pesticide formulation	Active ingredient conc. (g/L)	Formulation application rate (L/acre)	Experimental application rate (ng/cm^2)
Drexel® Chlorpyrifos 4E-AG	479	0.24	2800
Warrior II with Zeon Technology®	249	0.06	336
Steward® EC	150	0.33	1230

The average surface area of a dozen alfalfa leaves was determined to be 2.2 cm^2 and that area was used to calculate the pesticide mass needed to achieve the above application rates. Representing field conditions is important due to previous evidence that suggests extremely high application rates can result in increased rates of photodegradation.[64,66] Following application to each leaf, solvent was evaporated in the dark prior to irradiation for 15 minutes. Application reproducibility was examined and found to be consistent. With triplicate applications chlorpyrifos, lambda-cyhalothrin, and indoxacarb had relative standard deviations percentages of 5.1%, 10.0%, and 12.6%, respectively.

Irradiation

The spectrum of light produced by the SunTest CPS+, shown in Figure 9, was obtained using an Apogee PS-300 Spectroradiometer. Filters were used to cutoff wavelengths <280 nm to closely mirror the spectrum of sunlight that would be observed at the surface of the Earth.[71] The SunTest has previously been shown to be an effective mimic of natural sunlight.[72]

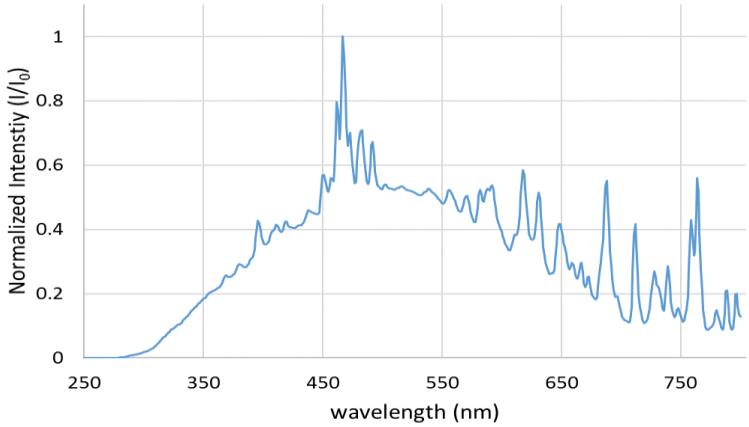

Figure 9. Spectrum of Light Produced by Atlas SunTest CPS+ Solar Simulator. I and I_0 represent the intensity of light at that wavenlength and the peak intensity for a single wavelength.

Following solvent evaporation, the sample tray was then placed back into the solar simulator which was set at 550 W m^{-2}. Samples were irradiated for up to 8 hours with samples being removed from the solar simulator at t= 0, 1, 2, 4, 6, and 8 hours. When samples were removed from the solar simulator, individual leaves were stored in glass vials at -20ºC until analysis. Dark controls were used to account for losses due to processes other than photodegradation, such as volatilization. The dark controls were also kept in the solar simulator; however, they were covered by aluminum foil to prevent them from being hit by the light produced. Similarly, to ensure that there was no transfer of pesticide from one leaf to another within the solar simulator, a leaf that received no pesticide was placed in the sample area and served as a blank. Cross-contamination in the solar simulator was not an issue for any of the experiments.

Actinometry

The p-nitroanisole/pyridine (PNA/pyridine) chemical actinometer was used to monitor fluctuations in light intensity during experiments.[73] Stock solutions of PNA in acetonitrile (10 mM) and pyridine in Milli-Q water (1 M) were made. In a dark environment prior to each experiment, these stock solutions were used to make one solution containing 10 µM PNA and 1 mM pyridine. This solution was then poured into quartz cuvettes which were placed in the solar simulator. An actinometry sample was removed from the solar simulator each time leaf samples were removed. A dark control was used for the actinometry samples by covering one cuvette in aluminum foil for the duration of irradiation.

PNA/pyridine samples were analyzed on a Shimadzu Prominence-i LC-2030C 3D with an Agilent Poroshell 120 EC-C18 column (4.6 mm x 100 mm x 2.7 µm). The mobile phase was 50:50 acetonitrile:water with a flow rate of 0.75mL/min. Peak areas were measured at 314 nm and the decrease in peak areas with respect to irradiation times were then used to monitor the intensity of light.

The PNA/pyridine actinometer used to monitor variations in light intensity showed that the light being produced within the solar simulator was consistent throughout all experiments at 550 W m^{-2}. The equations used for these calculations can be found in Laszakovits et al.[73]

Extraction

Prior to extraction, a solution containing isotope-labelled surrogate compounds was spiked onto each leaf at a concentration equal to the pesticide application to account for any losses throughout the extraction process. Chlorpyrifos-d10 was used as the surrogate for chlorpyrifos samples and tertbuthylazine-d5 was used as the surrogate for lambda-cyhalothrin and indoxacarb samples. 10 mL of reagent alcohol was then added to each glass vial and the vials were sonicated for 15 minutes using a Branson 1510 Ultrasonic Cleaner. The extracts were then concentrated to 1-2 mL under a gentle stream of nitrogen using an Biotage TurboVap II.

The extracts were a dark green color and required additional cleanup. 15 cm glass pipettes were packed with glass wool and then 0.6 grams of Florisil and 0.1 grams of graphitized carbon black (GCB). The packed columns were conditioned with 5 mL of hexane and then 5 mL of 4:1 hexane:acetone immediately prior to their use. The concentrated extracts were then added and eluted with an additional 15 mL of 4:1 hexane:acetone. Then the collected eluent was concentrated to ~300 µL using the Biotage TurboVap II. Spike and recovery experiments showed chlorpyrifos, lambda-cyhalothrin, and indoxacarb had recoveries of 78.9±4.0%, 85.9±8.6%, and 96.8±12.2% for the total extraction process, process.

GC-MS

Pesticides were quantified using a Thermo Fisher Scientific Trace 1310 Gas Chromatograph (GC) coupled to a TSQ 8000 Evo triple quadrupole mass spectrometer (MS). Separation was performed on a Phenomenex ZB-5MSplus (30 m long x 0.25 mm i.d. x 0.25 µm film thickness) fused silica capillary column with a 10-m deactivated guard column (Thermo Fisher Scientific). The inlet temperature was 300°C and injections were conducted in splitless mode. The

oven temperature program for chlorpyrifos was: 90°C (hold 0.5 min), ramp to 300°C at 15°C/min, hold at 300°C for 10 minutes. For lambda-cyhalothrin and indoxacarb, the oven temperature program was: 90°C (hold 0.5 min), ramp to 170°C at 15°C/min, ramp to 300°C at 9°C/min, hold at 300°C for 10 minutes. The MS was operated in electron ionization-selective reaction monitoring (EI-SRM) mode for chlorpyrifos and indoxacarb and in electron ionization-single ion monitoring (EI-SIM) for lambda-cyhalothrin. Target analyte retention times and SRM transitions are provided in Table 4. Concentrations were determined based on the ratio of the target analyte peak area to the corresponding surrogate peak area. An eight-point calibration curve was prepared from the peak area ratios of the target analyte to the corresponding surrogate for each pesticide

.

Table 4. Target Analyte Retention Times and Monitored Ions/Ion Transitions.

Compound	Retention time (min)	MS Quantitation ion/ion transition	MS Confirmation ion/ion transition 1	MS Confirmation ion/ion transition 2
Chlorpyrifos	11.16	314.0 / 258.0	286.0 / 257.9	316.0 / 259.9
Lambda-cyhalothrin	18.17	197.0	181.0	208.0
Indoxacarb	21.69	218.0 / 203.1	264.0 / 176.1	203.0 / 134.1
Chlorpyifos-d10	11.10	324.0 / 259.9	326.0 / 196.9	326.0 / 262.0
Tertbuthylazine-d5	10.46	178.0 / 143.0	219.0 / 137.0	219.0 / 76.0

Calculating photodegradation rates

The concentration of pesticide present on leaves, normalized against the initial concentration, with respect to irradiation time will be graphed and fit with an exponential line of the form in equation 18.

$$c_t = c_o e^{-k_{\text{photo}} t} \tag{18}$$

where c_t is the pesticide concentration at time t, c_0 is the initial pesticide concentration, k_{photo} is the pseudo-first order photodegradation rate constant, and t is irradiation time. We use the term 'pseudo-first order' when describing the rates because the nature of the decay is going to be dependent on the reaction conditions.[74]

After calculating these pseudo-first order rates, statistical analysis was conducted to determine if the rates for the active ingredient and formulation of each pesticide were statistically difference (with 95% confidence intervals).

Using Measured Photodegradation Rates in the PeDAL Model

The measured rates were used in the PeDAL model to further highlight the necessity for chemical-specific and location-specific photodegradation in environmental modeling. Since chlorpyrifos was used in the initial model evaluation, no further of this chemical occurred here.

Research on the dissipation of lambda-cyhalothrin and indoxacarb on leaves is limited, so only one scenario for each pesticide was modeled. A study by Seenivasan et al. that measured lambda-cyhalothrin residues on tea leaves in India was modeled to evaluate the lambda-cyhalothrin foliar photodegradation rate value.[75] This scenario used two locations in Tamil Nadu, India and each location used three plots with different application rates totaling six field trials. Since the two locations used were close to one another, DT_{50} values were calculated individually for all six field trials according to the guidelines of the Forum for the Coordination of pesticide fate models and their Use (FOCUS)[76] and were then averaged to obtain a DT_{50} that served as the measured value (Section A1).

A study by Sdeek et al. measuring pesticide residues on sugar beet leaves in the Giza Governorate of Egypt at different times after application was modeled to evaluate the indoxacarb

foliar photodegradation rate values found here.[77] Three plots at the same site had indoxacarb applied at different rates so the DT_{50} for each application was calculated and the average was used as the measured value.

For modeling both scenarios/pesticides, the obtained foliar photodegradation rate for the commercial formulation was used rather than the active ingredient. All input parameters related to meteorological and field conditions for all modeled scenarios are listed in Table A11. Input values

for related to the chemical properties of the pesticide are located in Table A1. Both of these scenarios were also modeled using no photodegradation to highlight the importance of this process and the need for future research attention in this area.

Results

Chlorpyrifos

The sample chamber was kept at a consistent 21ºC for the tests of the active ingredient and the commercial formulation; however, this still was not cool enough to prevent a large amount of volatilization. The dark controls for the active ingredient and the formulation contained <40% of the initial chlorpyrifos present (Figure 10). There was no statistical difference between the irradiated samples and the dark controls that were both removed from the solar simulator at the end of the experiment (t = 8 h). This demonstrates that photodegradation on alfalfa leaf surfaces is not be a major dissipation pathway for chlorpyrifos, which will be dominated by volatilization. This is supported by Walia et al. who observed only 30% degradation of chlorpyrifos on a soft-shield fern (*Polystichum setiferum*) after receiving 9 hours per day of simulated sunlight at a constant 1000 W m^{-2} for 25 days (dark control still had 95% of initial chlorpyrifos mass present).[29] Future modeling

for chlorpyrifos would likely be improved by using the rate that can be obtained from the data reported by Walia et al. since some degree of photodegradation is likely to place. However, ignoring photodegradation for chlorpyrifos would likely still lead to accurate results in most scenarios. This may be untrue for extreme scenarios with unusually strong sunlight and unusually low temperatures, preventing volatilizatio

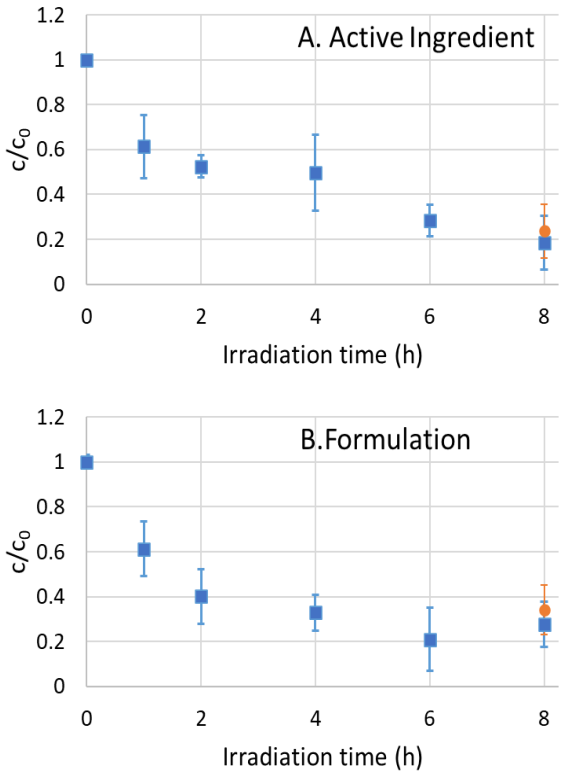

Figure 10. Foliar photodegradation of Chlorpyrifos on Alfalfa Leaves. (A) active ingredient and (B) formulation. Blue squares represent irradiated samples while orange circles represent the dark controls. Error bars represent the standard deviation of the triplicate measurement.

Lambda-cyhalothrin

The results of the photodegradation experiments for the lambda-cyhalothrin active ingredient and formulation are shown in Table 5 and Figure 11. The formulation did

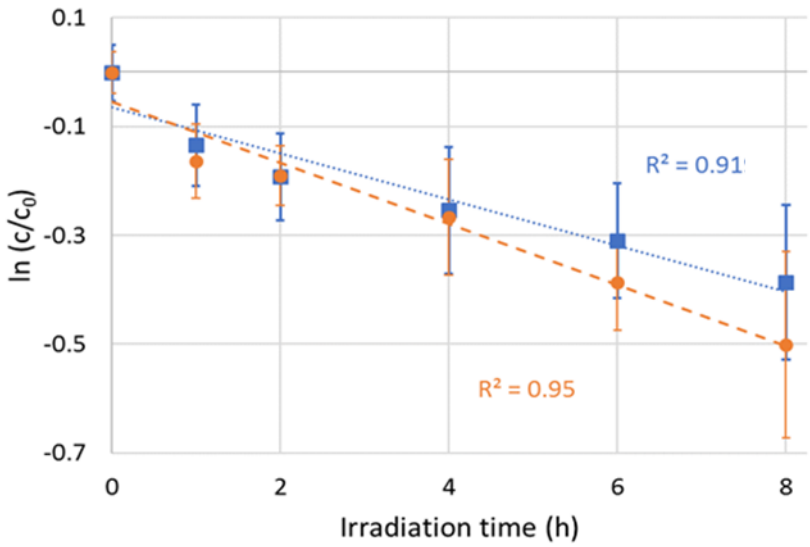

Figure 11. Foliar Photodegradation of Lambda-cyhalothrin on alfalfa leaves. Blue squares and the blue dotted line represent the active ingredient. Orange circles and the orange dashed line represents the commercial formulation. Error bars represent standard deviations on triplicate measurements and follow the same color code.

photodegrade slightly faster, however, there was no statistical difference between the formulation and the active ingredient. The dark concentrations in the dark controls were >90% the concentration of the samples that received no irradiation (t = 0 h) indicating the losses experienced in the irradiated samples can be predominantly attributed to photodegradation.

Table 5. Pseudo-first Order Roliar Photodegradation Rates for Lambda-cyhalothrin and Indoxacarb on Alfalfa Leaves with 95% Confidence Intervals

	Pseudo-first order foliar photodegradation rate constants (h^{-1})	
Chemical	Active ingredient	Formulation
Lambda-cyhalothrin	0.042±0.017	0.056±0.018
Indoxacarb	0.035±0.018	0.037±0.021

Indoxacarb

The results of the photodegradation experiments for the indoxacarb active ingredient and formulation are shown in Table 5 and Figure 12. There was no statistical difference between the

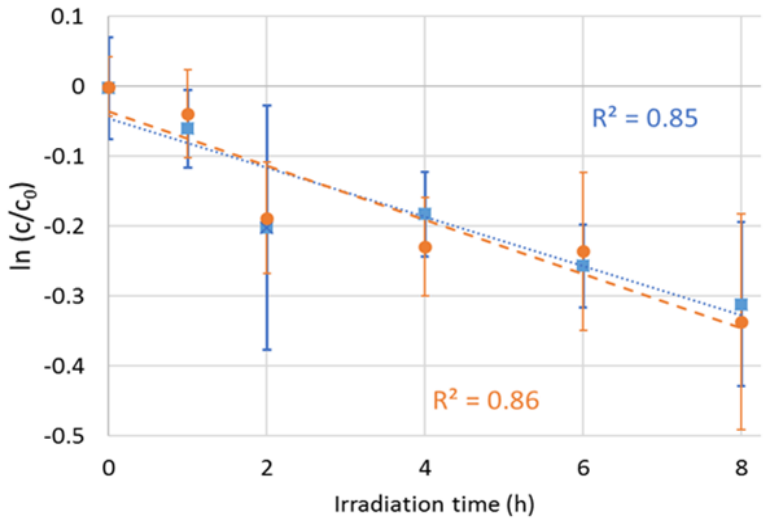

Figure 12. Foliar Photodegradation of Indoxacarb on Alfalfa Leaves. Blue squares and the blue dotted line represent the active ingredient. Orange circles and the orange dashed line represents the commercial formulation. Error bars represent standard deviations on triplicate measurements and follow the same color code.

rate of photodegradation for the active ingredient when compared to the commercial formulation. For both experiments the dark control contained over 90% of the original pesticide mass indicating that there were minimal losses due to processes other than photodegradation.

Using Measured Photodegradation Rates in the PeDAL model

Seenivasan et al. measured lambda-cyhalothrin residues following its application to tea leaves in two adjacent locations in Tamil Nadu, India.[75] Three application rates were used at each location. The DT_{50}, which was calculated according to the guidelines of FOCUS, was determined to be between 0.69-1.82 days depending on location and application rate. This is in good agreement with the modeled results produced by PeDAL for the same scenario. PeDAL predicted a DT_{50} of 1.20 days when using the photodegradation rate determined for the lambda-cyhalothrin formulation (DT_{50}=1.07-2.11 days when using the range reported for the photodegradation rate in Table 5).

Indoxacarb residues were measured by Sdeek et al. on sugar beet leaves following application in Dokki, Egypt.[77] The DT_{50} values that were calculated from the concentrations Sdeek et al. reported ranged from 1.23-1.67 days depending on the application rate used with an average DT_{50} value of 1.45 days. When the PeDAL model was used to simulate this same scenario, a DT_{50} value of 2.18 days (1.21-6.08 days when using the photodegradation rate range reported in Table 5) was predicted.

Deviation between modeled and measured results could be due to differences in the formulation composition used in each study. The presence of adjuvants/surfactants have been shown to impact pesticide fate processes, such as volatilization[61–63,78], photodegradation[64,65], and leaf penetration[31], when compared to the pure active ingredient. Given these effects, it is reasonable to suspect that differences in the adjuvants/surfactants used in different commercial formulations

could cause differences in photodegradation rates. The type of fruit wax used has also been shown to impact the rate of pesticide photodegradation by as much as a factor of five.[58] Similarly, differences in the surfaces of the alfalfa leaves used to determine the foliar photodegradation rate compared to the tea and sugar beet leaves used in the dissipation studies could also explain some of the discrepancy between modeled and measured results. Ideally, all photodegradation rates would be obtained on the same surface that is being modeled.

However, since the range of DT_{50} values predicted by the PeDAL model overlaps with the range of measured values for both scenarios, there appears to be good agreement between measured and modeled results. This is particularly encouraging for these two pesticides given that the predicted losses were attributed almost entirely to photodegradation with losses due to volatilization in the modeled scenarios totaling 0.3% and 0.0% for lambda-cyhalothrin and indoxacarb, respectively. When excluding photodegradation while modeling these scenarios, these pesticides would be expected to persist for an extremely long time. This illustrates the need for condition-specific photodegradation in modeling and suggests that the obtained foliar photodegradation rates for lambda-cyhalothrin and indoxacarb can be utilized as inputs in the PeDAL model to more accurately predict their post-application fate on leaves.

Conclusions

The measured pesticide foliar photodegradation rates for lambda-cyhalothrin and indoxacarb possess valuable potential in terms of their use in environmental fate models, such as the PeDAL model. These are some of the first pesticide photodegradation rates measured on the surface of actual leaves and thus, should offer more relevance in terms of environmental modeling than previously reported rates on extracted waxes. The results of the experiments with chlorpyrifos

support previous data suggesting that photodegradation is not a major dissipation process for the chemical. Future research should be directed towards expanding the list of pesticides photodegradation rates measured on leaf surfaces as this study appears to be one of less than a half dozen. Additionally, determining photodegradation products is also an important area to focus on since the photodegradation product could still be toxicologically relevant. This is particularly important to ensure that the photodegradation product is not more toxic than the parent pesticide.

CHAPTER 4: CONCLUSIONS

General Conclusions

Understanding pesticide fate following application to planted fields will allow for successful management of pests, protection of beneficial insects, and thus, hopefully, increased crop yields with minimal adverse effects on the environment. The environmental fate of a pesticide is going to depends heavily on its own physicochemical properties, the characteristics of the field to which it is applied, and the meteorological conditions it is subjected to following application.

The Pesticide Dissipation from Agricultural Land (PeDAL) model was developed to accurately simulate pesticide fate. I developed this model by incorporating a foliar photodegradation component that was chemical- and location-specific to a pre-existing module for calculating pesticide volatilization from plants and/or soil, the Pesticide Loss via Volatilization (PLoVo) model. The photodegradation component includes a module (Bird's Clear Sky Model) for predicting hourly sunlight intensities for any location on Earth.[30] These radiation predictions combined with kinetics data from the literature on pesticide photodegradation on leaf surfaces allows for factors related to the pesticide and location/timing to be considered when estimating foliar photodegradation. This allows for a more realistic prediction of environmental fate than what is achieved using previous environmental fate models. The volatilization component is based on multiphase partitioning and Fick's Law of Diffusion. A generic foliar penetration component was also added to the PeDAL model.

The model calculates the time required to reach half of the pesticide's concentration immediately after application (DT_{50}). Other outputs include estimated pesticide concentrations in the soil and plant compartments with respect to time after application, emission flux values that can be used for atmospheric modeling purposes, and specified contributions by volatilization and photodegradation to the overall dissipation.

I evaluated the model by simulating scenarios described in pesticide dissipation studies in the literature and then comparing the DT_{50} values predicted by the PeDAL model with the measured values that had been reported. There was good agreement between modeled and measured DT_{50} values (n = 49, R^2 = 0.76, RMSE = 0.94 days). Various aspects of pesticide dissipation were then examined using the PeDAL model.

First, I conducted two separate sensitivity analyses to examine the influence of photodegradation on pesticide dissipation. The first sensitivity analysis was a simulation for over 3000 hypothetical chemicals with three degrees of photodegradation. Using chemical space diagrams and the results of these simulations, I was able to highlight the region of chemicals that will have their overall dissipation most dependent on their photoreactivity. The second sensitivity analysis was used to highlight the benefits of the newly developed foliar photodegradation component, specifically relative to the traditional method for computing pesticide photodegradation on leaves in environmental modeling. Two application timings for five locations were used to illustrate how dissipation can vary widely depending on the location and timing of the application, two factors often overlooked in past modeling efforts. This analysis also demonstrated the degree to which using a generic, constant photodegradation rate can incorrectly predict photodegradation.

Questions related to the impact of application timing on pesticide dissipation were then examined. Simulations showed that the time of day and time of year of application both can have impacts on the pesticide dissipation rate and DT_{50}. Finally, the ability of the PeDAL model to accurately predict an emission flux was evaluated by comparing modeled and measured fluxes for two scenarios reported in the literature. The results of this comparison suggested the PeDAL model has the potential to be a valuable resource that can predict emission fluxes as inputs for an atmospheric dispersion model.

Due to the lack of chemical-specific data related to pesticide photodegradation on leaf surfaces, the PeDAL model is limited in its applicability. To expand its potential usage, I conducted a series of pesticide photodegradation experiments using an Atlas SunTest CPS+ solar simulator. Due to our source of funding, these experiments were carried out on alfalfa leaves with alfalfa-related pesticides (active ingredients = chlorpyrifos, lambda-cyhalothrin, and indoxacarb).

The first step of these experiments was to determine the intensity of light being produced in the solar simulator and to make sure it was consistent and representative of natural sunlight. The spectrum of light produced was measured using a spectroradiometer and I monitored the intensity with the p-nitroanisole/pyridine (PNA/pyridine) chemical actinometer. The actinometry samples were analyzed using HPLC-UV/Vis and indicated that the light was consistent at 550 W/m^2.

I also conducted spike and recovery experiments to ensure efficient recovery of analytes. The extraction method utilized sonication in methanol, external column clean-up, and concentration under a stream of nitrogen. Isotopically labelled surrogates were used to account for analyte loss during the entire extraction process.

Irradiation experiments were then conducted for each of the pesticides listed earlier. Experiments were run for each pesticide as pure active ingredient and as part of a commercial formulation like what would be sprayed by farmers. The chlorpyrifos experiments indicated that photodegradation will be a very minor dissipation process. This supports previously reported data that demonstrated that chlorpyrifos foliar photodegradation is a relatively slow process that has a negligible impact on dissipation.[29] Pseudo-first order foliar photodegradation rates were obtained for the active ingredient and commercial formulation of lambda-cyhalothrin and indoxacarb. Lambda-cyhalothrin had rates of $0.042 \pm 0.017\ h^{-1}$ and $0.056 \pm 0.018\ h^{-1}$ for the active ingredient and formulation, respectively. Pure indoxacarb degraded at a rate of $0.035 \pm 0.018\ h^{-1}$ while formulated indoxacarb had a photodegradation rate of $0.037 \pm 0.021\ h^{-1}$. For both lambda-cyhalothrin and

indoxacarb there was no statistically significant difference between the photodegradation of the pure chemical and the formulated version.

These foliar photodegradation rates were then used as inputs in the PeDAL model to simulate two dissipation studies reported in the literature. Once again, there was a good agreement between the modeled and measured DT_{50} values.

Recommendations

Currently the major limiting factor in the potential use of the PeDAL model is the lack of photodegradation rates for pesticides on leaf surfaces reported in the literature. As I have shown, foliar pesticide photodegradation is a critical process to account for in predicting pesticide dissipation following application. Without more of these rates, proper environmental fate modeling cannot be performed for most pesticides used. Thus, the area I would suggest future research focus on is obtaining more foliar photodegradation rates. Ideally, these experiments would be conducted on the same type of leaf surface that is being modeled to account for any potential surface-related effects on photodegradation. Similarly, these experiments should be performed using the commercial formulation that is being sprayed so that the influence of adjuvants and other ingredients can be accounted for. The results of the sensitivity analysis discussed in Chapter 2 can drive the focus of which pesticides to study by identifying the minimally or non-volatile pesticides that will have their dissipation dominated by photodegradation.

The PeDAL model itself also needs to be further evaluated to ensure its ability to predict pesticide dissipation. Due to the necessity to estimate many input parameters during the model evaluation, dissipation studies with more specific input parameters should be conducted to allow

for the better examination of the model's performance. Ideally these studies would use a variety of locations, timings, and pesticides to evaluate the model under a wide range of conditions.

To improve the model's ability to accurately predict volatilization, more plant-pesticide combination specific plant-air equations should be measured. Conducting experiments that would allow for foliar penetration to be changed from a generic component to a chemical-plant specific process would also likely improve the accuracy of the PeDAL model. However, given that penetration is a minor process compared to volatilization and photodegradation, this work should not be prioritized. Instead, it would likely be better to spend resources in the pursuit of adding additional components to the model, such as a wash-off module. Currently the model is only designed to work in scenarios with no precipitation but adding a wash-off module would allow for expanded applicability of the model.

Finally, to allow for farmers to protect beneficial insects while effectively managing pests, toxicity thresholds should be input into the model. This will allow pesticide applicators to have a better idea of how long their pesticide is effective against the given pest and when it would be safe to introduce beneficial insects, like pollinators, into the field.

REFERENCES

(1) Damalas, C. A. Understanding Benefits and Risks of Pesticide Use. *Sci. Res. Essays* **2009**, *4* (10), 945–949.

(2) DDT - A Brief History and Status | Ingredients Used in Pesticide Products | US EPA https://www.epa.gov/ingredients-used-pesticide-products/ddt-brief-history-and-status (accessed Mar 18, 2021).

(3) Aktar, W.; Sengupta, D.; Chowdhury, A. Impact of Pesticides Use in Agriculture: Their Benefits and Hazards. *Interdiscip. Toxicol.* **2009**, *2* (1), 1–12. https://doi.org/10.2478/v10102-009-0001-7.

(4) Maksymiv, I. Pesticides: Benefits and Hazards. *J. Vasyl Stefanyk Precarpathian Natl. Univ.* **2015**, *2* (1), 70–76. https://doi.org/10.15330/jpnu.2.1.70-76.

(5) Cooper, J.; Dobson, H. The Benefits of Pesticides to Mankind and the Environment. *Crop Prot.* **2007**, *26* (9), 1337–1348. https://doi.org/10.1016/j.cropro.2007.03.022.

(6) Atwood, D.; Paisley-Jones, C. *2008-2012 Market Estimates*; 2017.

(7) Nicolopoulou-Stamati, P.; Maipas, S.; Kotampasi, C.; Stamatis, P.; Hens, L. Chemical Pesticides and Human Health: The Urgent Need for a New Concept in Agriculture. *Front. Public Heal.* **2016**, *4* (July), 1–8. https://doi.org/10.3389/fpubh.2016.00148.

(8) Hawkins, N. J.; Bass, C.; Dixon, A.; Neve, P. The Evolutionary Origins of

Pesticide Resistance. *Biol. Rev.* **2019**, *94* (1), 135–155. https://doi.org/10.1111/brv.12440.

(9) Miglani, R.; Bisht, S. S. World of Earthworms with Pesticides and Insecticides. *Interdiscip. Toxicol.* **2020**, *12* (2), 71–82. https://doi.org/10.2478/intox-2019-0008.

(10) Can't Live Without Me | The Adventures of Herman the Worm | U of I Extension https://web.extension.illinois.edu/worms/live/ (accessed Mar 21, 2021).

(11) Hageman, K. J.; Bogdal, C.; Scheringer, M. Chapter 11 - Long-Range and Regional Atmospheric Transport of POPs and Implications for Global Cycling. In *Persistent Organic Pollutants (POPs): Analytical Techniques, Environmental Fate and Biological Effects*; Zhang, E. Y., Ed.; Elsevier: Waltham, MA, 2015; pp 363–387.

(12) Wania, F.; Mackay, D. Global Fractionation and Cold Condensation of Low Volatility Organochlorine Compounds in Polar Regions. *Ambio* **1993**, *22* (1), 10–18. https://doi.org/10.2307/4314030.

(13) Macaulay, S. J.; Hageman, K. J.; Alumbaugh, R. E.; Lyons, S. M.; Piggott, J. J.; Matthaei, C. D. Chronic Toxicities of Neonicotinoids to Nymphs of the Common New Zealand Mayfly Deleatidium Spp. *Environ. Toxicol. Chem.* **2019**. https://doi.org/10.1002/etc.4556.

(14) Muth, F.; Leonard, A. S. A Neonicotinoid Pesticide Impairs Foraging, but Not Learning, in Free-Flying Bumblebees. *Sci. Rep.* **2019**, *9* (1), 1–13. https://doi.org/10.1038/s41598-019-39701-5.

(15) Lu, C.; Warchol, K. M.; Callahan, R. A. Sub-Lethal Exposure to Neonicotinoids Impaired Honey Bees Winterization before Proceeding to Colony Collapse Disorder. *Bull. Insectology* **2014**, *67* (1), 125–130.

(16) Berheim, E. H.; Jenks, J. A.; Lundgren, J. G.; Michel, E. S.; Grove, D.; Jensen, W. F. Effects of Neonicotinoid Insecticides on Physiology and Reproductive Characteristics of Captive Female and Fawn White-Tailed Deer. *Sci. Rep.* **2019**, *9* (1), 1–10. https://doi.org/10.1038/s41598-019-40994-9.

(17) Hites, R. A. The Rise and Fall of Chlorpyrifos in the United States. *Environ. Sci. Technol.* **2021**, *55* (3), 1354–1358. https://doi.org/10.1021/acs.est.0c06579.

(18) DDT Regulatory History: A Brief Survey (to 1975) | About EPA | US EPA https://archive.epa.gov/epa/aboutepa/ddt-regulatory-history-brief-survey-1975.html (accessed Mar 20, 2021).

(19) Sarmah, A. K.; Müller, K.; Ahmad, R. Fate and Behaviour of Pesticides in the Agroecosystem - A Review with a New Zealand Perspective. *Aust. J. Soil Res.* **2004**, *42* (2), 125–154. https://doi.org/10.1071/SR03100.

(20) Fantke, P.; Juraske, R. Variability of Pesticide Dissipation Half-Lives in Plants. *Environ. Sci. Technol.* **2013**, *47*, 3548–3562. https://doi.org/10.1021/es303525x.

(21) Taylor, M. R.; Lyons, S. M.; Davie-Martin, C. L.; Geoghegan, T. S.; Hageman, K. J. Understanding Trends in Pesticide Volatilization from Agricultural Fields Using the Pesticide Loss via Volatilization (PLoVo) Model. *Environ. Sci. Technol.* **2019**, *54* (4), 2202–2209. https://doi.org/10.1021/acs.est.9b04762.

(22) van den Berg, F.; Jacobs, C. M. J.; Butler Ellis, M. C.; Spanoghe, P.; Doan Ngoc, K.; Fragkoulis, G. Modelling Exposure of Workers, Residents and Bystanders to Vapour of Plant Protection Products after Application to Crops. *Sci. Total Environ.* **2016**, *573*, 1010–1020. https://doi.org/10.1016/j.scitotenv.2016.08.180.

(23) Houbraken, M.; Doan Ngoc, K.; van den Berg, F.; Spanoghe, P. Modelling Pesticides Volatilisation in Greenhouses: Sensitivity Analysis of a Modified PEARL Model. *Sci. Total Environ.* **2017**, *599–600*, 1408–1416. https://doi.org/10.1016/j.scitotenv.2017.05.027.

(24) van den Berg, F.; Tiktak, A.; Boesten, J. J. T. I.; van der Linden, A. M. A. *PEARL Model for Pesticide Behaviour and Emissions in Soil-Plant System: Description of Processes*; 2016; Vol. 61. https://doi.org/ISSN 1566-7197.

(25) Lichiheb, N.; Personne, E.; Bedos, C.; Van den Berg, F.; Barriuso, E. Implementation of the Effects of Physicochemical Properties on the Foliar Penetration of Pesticides and Its Potential for Estimating Pesticide Volatilization from Plants. *Sci. Total Environ.* **2016**, *550*, 1022–1031. https://doi.org/10.1016/j.scitotenv.2016.01.058.

(26) Lichiheb, N.; Personne, E.; Bedos, C.; Barriuso, E. Adaptation of a Resistive Model to Pesticide Volatilization from Plants at the Field Scale: Comparison with a Dataset. *Atmos. Environ.* **2014**, *83*, 260–268. https://doi.org/10.1016/j.atmosenv.2013.11.004.

(27) Wolters, A.; Leistra, M.; Linnemann, V.; Klein, M.; Schäffer, A.; Vereecken, H. Pesticide Volatilization from Plants: Improvement of the PEC Model PELMO

Based on a Boundary-Layer Concept. *Environ. Sci. Technol.* **2004**, *38* (10), 2885–2893. https://doi.org/10.1021/es035061m.

(28) Monadjemi, S.; Ter Halle, A.; Richard, C. Accelerated Dissipation of the Herbicide Cycloxydim on Wax Films in the Presence of the Fungicide Chlorothalonil and under the Action of Solar Light. *J. Agric. Food Chem.* **2014**, *62* (21), 4846–4851. https://doi.org/10.1021/jf500771s.

(29) Walia, S.; Dureja, P.; Mukerjee, S. K. New Photodegradation Products of Chlorpyrifos and Their Detection on Glass, Soil, and Leaf Surfaces. *Arch. Environ. Contam. Toxicol.* **1988**, *17*, 183–188.

(30) Bird, R. E.; Hulstrom, R. L. *A Simplified Clear Sky Model for Direct and Diffuse Insolation on Horizontal Surfaces*; 1981. https://doi.org/10.2172/6510849.

(31) Lichiheb, N.; Bedos, C.; Personne, E.; Benoit, P.; Bergheaud, V.; Fanucci, O.; Bouhlel, J.; Barriuso, E. Measuring Leaf Penetration and Volatilization of Chlorothalonil and Epoxiconazole Applied on Wheat Leaves in a Laboratory-Scale Experiment. *J. Environ. Qual.* **2015**, *44*, 1782–1790. https://doi.org/10.2134/jeq2015.03.0165.

(32) Lyons, S. M.; Hageman, K. J. Foliar Photodegradation in Pesticide Fate Modeling: Development & Evaluation of the Pesticide Dissipation from Agricultural Land (PeDAL) Model. *Environ. Sci. Technol.* **2021**.

(33) Damalas, C. A.; Eleftherohorinos, I. G. Pesticide Exposure, Safety Issues, and Risk Assessment Indicators. *Int. J. Environ. Res. Public Health* **2011**, *8* (5), 1402–1419. https://doi.org/10.3390/ijerph8051402.

(34) van den Berg, F.; Tiktak, A.; Boesten, J. J. T. I.; van der Linden, A. M. A. *PEARL Model for Pesticide Behaviour and Emissions in Soil-Plant System: Description of Processes.*; 2016; Vol. 61.

(35) Fantke, P.; Gillespie, B. W.; Juraske, R.; Jolliet, O. Estimating Half-Lives for Pesticide Dissipation from Plants. *Environ. Sci. Technol.* **2014**, *48*, 8588–8602. https://doi.org/10.1021/es500434p.

(36) Pao, K. C. H. Residue Studies of Phoxim (Baythion) on Tea Bushes. *Acta Entomol. Sin.* **1975**, *18* (2), 140.

(37) EPA, U. S. *Pesticides Abstracts*; Washington D.C., 1976.

(38) Air Quality Dispersion Modeling - Alternative Models | Support Center for Regulatory Atmospheric Modeling (SCRAM) | US EPA https://www.epa.gov/scram/air-quality-dispersion-modeling-alternative-models#isc3 (accessed Aug 12, 2019).

(39) Davie-Martin, C. L.; Hageman, K. J.; Chin, Y. P. An Improved Screening Tool for Predicting Volatilization of Pesticides Applied to Soils. *Environ. Sci. Technol.* **2013**, *47*, 868–876. https://doi.org/10.1021/es3020277.

(40) Leistra, M.; Smelt, J. H.; Hilbrand Weststrate, J.; Van Den Berg, F.; Aalderink, R. Volatilization of the Pesticides Chlorpyrifos and Fenpropimorph from a Potato Crop. *Environ. Sci. Technol.* **2006**, *40* (1), 96–102. https://doi.org/10.1021/es051248x.

(41) Pick, F. E.; Van Dyk, L. P.; De Beer, P. R. The Effect of Simulated Rain on

Deposits of Some Cotton Pesticides. *Pestic. Sci.* **1984**, *15* (6), 616–623. https://doi.org/10.1002/ps.2780150614.

(42) Linders, J.; Mensink, H.; Stephenson, G.; Wauchope, D.; Racke, K. *Foliar Interception and Retention Values after Pesticide Application. A Proposal for Standardized Values for Environmental Risk Assessment (Technical Report)*; 2000; Vol. 72. https://doi.org/10.1351/pac200072112199.

(43) Davie-Martin, C. L.; Hageman, K. J.; Chin, Y. P.; Rougé, V.; Fujita, Y. Influence of Temperature, Relative Humidity, and Soil Properties on the Soil-Air Partitioning of Semivolatile Pesticides: Laboratory Measurements and Predictive Models. *Environ. Sci. Technol.* **2015**, *49*, 10431–10439. https://doi.org/10.1021/acs.est.5b02525.

(44) Schwarzenbach, R. P.; Gschwend, P. M.; Imboden, D. M. *Environmental Organic Chemistry*, 2nd ed.; John Wiley & Sons, Inc.: Hoboken, New Jersey, 2003.

(45) Nobel, P. S. Temperature and Energy Budgets. In *Physicochemical and Environmental Plant Physiology*; 2007; pp 307–350. https://doi.org/10.1016/b978-012520026-4/50008-1.

(46) Komp, P.; McLachlan, M. S. Influence of Temperature on the Plant/Air Partitioning of Semivolatile Organic Compounds. *Environ. Sci. Technol.* **1997**, *31*, 886–890.

(47) Su, L.; Sivey, J. D.; Dai, N. Emerging Investigator Series: Sunlight Photolysis of 2,4-D Herbicides in Systems Simulating Leaf Surfaces. *Environ. Sci. Process. Impacts* **2018**, *20*, 1123–1135. https://doi.org/10.1039/c8em00186c.

(48) Eyheraguibel, B.; Richard, C.; Ledoigt, G.; Ter Halle, A. Photoprotection by Plant Extracts: A New Ecological Means to Reduce Pesticide Photodegradation. *J. Agric. Food Chem.* **2010**, *58* (17), 9692–9696. https://doi.org/10.1021/jf101792h.

(49) Monadjemi, S.; El Roz, M.; Richard, C.; Ter Halle, A. Photoreduction of Chlorothalonil Fungicide on Plant Leaf Models. *Environ. Sci. Technol.* **2011**, *45* (22), 9582–9589. https://doi.org/10.1021/es202400s.

(50) Fukushima, M.; Katagi, T. Photodegradation of Fenitrothion and Parathion in Tomato Epicuticular Waxes. *J. Agric. Food Chem.* **2006**, *54* (2), 474–479. https://doi.org/10.1021/jf052113d.

(51) Anderson, S. C.; Chu, L.; Bouma, C.; Beukelman, L.; McLouth, R.; Larson, E.; Nienow, A. M. Comparison of the Photodegradation of Imazethapyr in Aqueous Solution, on Epicuticular Waxes, and on Intact Corn (Zea Mays) and Soybean (Glycine Max) Leaves. *J. Environ. Sci. Heal. - Part B Pestic. Food Contam. Agric. Wastes* **2019**, *54* (2), 129–137. https://doi.org/10.1080/03601234.2018.1511400.

(52) Bird Clear Sky Model | Grid Modernization | NREL https://www.nrel.gov/grid/solar-resource/clear-sky.html (accessed Aug 26, 2020).

(53) Matuszko, D. Influence of the Extent and Genera of Cloud Cover on Solar Radiation Intensity. *Int. J. Climatol.* **2012**, *32*, 2403–2414. https://doi.org/10.1002/joc.2432.

(54) Komp, P.; Mclachlan, M. S. Interspecies Variability of the Plant/Air Partitioning of Polychlorinated Biphenyls. *Environ. Sci. Technol.* **1997**, *31* (10), 2944–2948. https://doi.org/10.1021/es970141+.

(55) van den Berg, F.; Bor, G.; Smidt, R. A.; van de Peppel-Groen, A. E.; Smelt, J. H.; Muller, T.; Maurer, T. *Volatilization of Parathion and Chlorothalonil after Spraying onto a Potato Crop*; Wageningen, Netherlands, 1995.

(56) Guth, J. A.; Reischmann, F. J.; Allen, R.; Arnold, D.; Hassink, J.; Leake, C. R.; Skidmore, M. W.; Reeves, G. L. Volatilisation of Crop Protection Chemicals from Crop and Soil Surfaces under Controlled Conditions-Prediction of Volatile Losses from Physico-Chemical Properties. *Chemosphere* **2004**, *57* (8), 871–887. https://doi.org/10.1016/j.chemosphere.2004.08.011.

(57) Rüdel, H. Volatilisation of Pesticides from Soil and Plant Surfaces. *Chemosphere* **1997**, *35* (1–2), 143–152. https://doi.org/10.1016/S0045-6535(97)00146-X.

(58) Cabras, P.; Angioni, A.; Garau, V. L.; Melis, M.; Pirisi, F. M.; Minelli, E. V. Effect of Epicuticular Waxes of Fruits on the Photodegradation of Fenthion. *J. Agric. Food Chem.* **1997**, *45* (9), 3681–3683. https://doi.org/10.1021/jf970102h.

(59) Tolls, J.; McLachlan, M. S. Partitioning of Semivolatile Organic Compounds between Air and Lolium Multlflorum (Welsh Ray Grass). *Environ. Sci. Technol.* **1994**, *28* (1), 159–166. https://doi.org/10.1021/es00050a022.

(60) Houbraken, M.; Senaeve, D.; Dávila, E. L.; Habimana, V.; De Cauwer, B.; Spanoghe, P.; Fevery, D.; Spanoghe, P. Influence of Adjuvants on the Dissipation of Fenpropimorph, Pyrimethanil, Chlorpyrifos and Lindane on the Solid/Gas Interface. *Sci. Total Environ.* **2015**, *138*, 357–363. https://doi.org/10.1016/j.chemosphere.2015.06.040.

(61) Houbraken, M.; Senaeve, D.; Dávila, E. L.; Habimana, V.; De Cauwer, B.;

Spanoghe, P. Formulation Approaches to Reduce Post-Application Pesticide Volatilisation from Glass Surfaces. *Sci. Total Environ.* **2018**, *633*, 728–737. https://doi.org/10.1016/j.scitotenv.2018.03.186.

(62) Das, S.; Hageman, K. J. Influence of Adjuvants on Pesticide Soil-Air Partition Coefficients: Laboratory Measurements and Predicted Effects on Volatilization. *Environ. Sci. Technol.* **2020**, *54* (12), 7302–7308. https://doi.org/10.1021/acs.est.0c00964.

(63) Stevens, P. J. G.; Bukovac, M. J. Studies on Octylphenoxy Surfactants. Part 1: Effects of Oxyethylene Content on Properties of Potential Relevance to Foliar Absorption. *Pest Manag. Sci.* **1987**, *20* (1), 19–35.

(64) Eyheraguibel, B.; ter Halle, A.; Richard, C. Photodegradation of Bentazon, Clopyralid, and Triclopyr on Model Leaves: Importance of a Systematic Evaluation of Pesticide Photostability on Crops. *J. Agric. Food Chem.* **2009**, *57*, 1960–1966.

(65) ter Halle, A.; Lavieille, D.; Richard, C. The Effect of Mixing Two Herbicides Mesotrione and Nicosulfuron on Their Photochemical Reactivity on Cuticular Wax Film. *Chemosphere* **2010**, *79*, 482–487. https://doi.org/10.1016/j.chemosphere.2010.01.003.

(66) Delphine, L.; Alexandra, T. H.; Bussiere, P. O.; Claire, R. Effect of a Spreading Adjuvant on Mesotrione Photolysis on Wax Films. *J. Agric. Food Chem.* **2009**, *57* (20), 9624–9628. https://doi.org/10.1021/jf901996d.

(67) Brenneman, T. B.; Sumner, H. R.; Harrison, G. W. Deposition and Retention of

Chlorothalonil Applied to Peanut Foliage: Effects of Application Methods, Fungicide Formulations and Oil Additives 1 . *Peanut Sci.* **1990**, *17* (2), 80–84. https://doi.org/10.3146/i0095-3679-17-2-9.

(68) Zhang, Z. Y.; Zhang, C. Z.; Liu, X. J.; Hong, X. Y. Dynamics of Pesticide Residues in the Autumn Chinese Cabbage (Brassica Chinensis L.) Grown in Open Fields. *Pest Manag. Sci.* **2006**, *62*, 350–355. https://doi.org/10.1002/ps.1174.

(69) Das, S.; Hageman, K. J.; Taylor, M.; Michelsen-heath, S.; Stewart, I. Fate of the Organophosphate Insecticide , Chlorpyrifos , in Leaves , Soil , and Air Following Application. *Chemosphere* **2020**, *243*, 125194. https://doi.org/10.1016/j.chemosphere.2019.125194.

(70) FAOSTAT http://www.fao.org/faostat/en/#data/RP (accessed Feb 3, 2021).

(71) Ultraviolet (UV) Radiation | UCAR Center for Science Education https://scied.ucar.edu/ultraviolet-uv-radiation (accessed Feb 3, 2021).

(72) Weber, J.; Halsall, C. J.; Wargent, J. J.; Paul, N. D. A Comparative Study on the Aqueous Photodegradation of Two Organophosphorus Pesticides under Simulated and Natural Sunlight. *J. Environ. Monit.* **2009**, *11* (3), 654–659. https://doi.org/10.1039/b811387d.

(73) Laszakovits, J. R.; Berg, S. M.; Anderson, B. G.; O'Brien, J. E.; Wammer, K. H.; Sharpless, C. M. P-Nitroanisole/Pyridine and p-Nitroacetophenone/Pyridine Actinometers Revisited: Quantum Yield in Comparison to Ferrioxalate. *Environ. Sci. Technol. Lett.* **2017**, *4* (1), 11–14. https://doi.org/10.1021/acs.estlett.6b00422.

(74) Logan, S. R. Does a Photochemical Reaction Have a Kinetic Order? *J. Chem. Educ.* **1997**, *74* (11), 1303. https://doi.org/10.1021/ed082p37.2.

(75) Seenivasan, S.; Muraleedharan, N. N. Residues of Lambda-Cyhalothrin in Tea. *Food Chem. Toxicol.* **2009**, *47* (2), 502–505. https://doi.org/10.1016/j.fct.2008.12.010.

(76) FOCUS. *Guidance Document on Estimating Persistence and Degradation Kinetics from Environmental Fate Studies on Pesticides in EU Registration*; 2006.

(77) Sdeek, F. A.; Taha, H. S. Indoxacarb Residue Analysis, Dissipation and Field Efficacy on Sugar Beet Applied for Spodoptera Littoralis Infestation. *Egypt. Sci. J. Pestic.* **2018**, *4* (1), 7–12.

(78) Houbraken, M.; Senaeve, D.; Fevery, D.; Spanoghe, P. Influence of Adjuvants on the Dissipation of Fenpropimorph, Pyrimethanil, Chlorpyrifos and Lindane on the Solid/Gas Interface. *Chemosphere* **2015**, *138*, 357–363. https://doi.org/10.1016/j.chemosphere.2015.06.040.

(79) EPA, U. S. Estimation Programs Interface Suite™ for Microsoft® Windows. United States Environmental Protection Agency: Washington, DC, USA 2019.

(80) Seker, H.; Yolcu, H.; Acikgoz, E. Primary Growth Parameters of Three Alfalfa Cultivars Adapted to Highland Climatic Conditions. *J. Agron. Crop Sci.* **2015**, *201* (3), 219–227. https://doi.org/10.1111/jac.12105.

(81) Turrell, F. M. A Quantitative Morphological Analysis of Large and Small Leaves of Alfalfa, with Special Reference to Internal Surface Author(S). *Source Am. J.*

Bot. **1942**, *29* (5), 400–415.

(82) Glenn, D. M. Canopy Gas Exchange and Water Use Efficiency of 'Empire' Apple in Response to Particle Film, Irrigation, and Microclimatic Factors. *J. Am. Soc. Hortic. Sci.* **2010**, *135* (1), 25–32. https://doi.org/10.21273/jashs.135.1.25.

(83) Shabani, A.; Ghaffary, K. A.; Sepaskhah, A. R.; Kamgar-Haghighi, A. A. Using the Artificial Neural Network to Estimate Leaf Area. *Sci. Hortic. (Amsterdam).* **2017**, *216*, 103–110. https://doi.org/10.1016/j.scienta.2016.12.032.

(84) Schechter, I.; Proctor, J. T. A.; Elfving, D. C. Morphological Differences among Apple Leaf Types. *HortScience* **1992**, *27* (2), 101–103. https://doi.org/10.21273/hortsci.27.2.101.

(85) Riikonen, J.; Kets, K.; Darbah, J.; Oksanen, E.; Sober, A.; Vapaavuori, E.; Kubiske, M. E.; Nelson, N.; Karnosky, D. F. Carbon Gain and Bud Physiology in Populus Tremuloides and Betula Papyrifera Grown under Long-Term Exposure to Elevated Concentrations of CO2 and O3. *Tree Physiol.* **2008**, *28* (2), 243–254. https://doi.org/10.1093/treephys/28.2.243.

(86) How Aspens Grow https://www.fs.fed.us/wildflowers/beauty/aspen/grow.shtml (accessed May 23, 2020).

(87) Heiskanen, J. Estimating Aboveground Tree Biomass and Leaf Area Index in a Mountain Birch Forest Using ASTER Satellite Data. *Int. J. Remote Sens.* **2006**, *27* (6), 1135–1158. https://doi.org/10.1080/01431160500353858.

(88) *Paper Birch (Betula Papyrifera).*

(89) Oksanen, E.; Riikonen, J.; Kaakinen, S.; Holopainen, T.; Vapaavuori, E. Structural Characteristics and Chemical Composition of Birch (Betula Pendula) Leaves Are Modified by Increasing CO2 and Ozone. *Glob. Chang. Biol.* **2005**, *11* (5), 732–748. https://doi.org/10.1111/j.1365-2486.2005.00938.x.

(90) Campillo, C.; García, M. I.; Daza, C.; Prieto, M. H. Study of a Non-Destructive Method for Estimating the Leaf Area Index in Vegetable Crops Using Digital Images. *HortScience* **2010**, *45* (10), 1459–1463.

(91) Pérez, R. A.; Brito, J. D.; Guerra, Y. R.; Re, S. S. Morphophysiological Indicators of Cabbage (Brassica Oleracea L. Var. Capitata) Planted Inside and Outside Greenhouse, under Ecuadorian Amazon Conditions. *J. Agric. Ecol. Res. Int.* **2015**, *3* (4), 160–167. https://doi.org/10.9734/jaeri/2015/16923.

(92) Jun, T.; Dongming, L. I. U.; Zezhou, L. I. U.; Limei, Y.; Zhiyuan, F.; Yumei, L. I. U.; Mu, Z. Preliminary Study of the Characteristics of Several Glossy Cabbage (Brassica Oleracea Var . Capitata L .) Mutants. *Hortic. Plant J.* **2015**, *1* (2), 93–100. https://doi.org/10.16420/j.issn.2095-9885.2015-0009.

(93) Munthali, D. C.; Tshegofatso, A. B. Factors Affecting Abundance and Damage Caused by Cabbage Aphid, Brevicoryne Brassicae on Four Brassica Leafy Vegetables: Brassica Oleracea Var. Acephala, B. Chinense, B. Napus and B. Carinata. *Open Entomol. J.* **2014**, *8* (1), 1–9. https://doi.org/10.2174/1874407901408010001.

(94) Pilau, F. G.; Angelocci, L. R. Leaf Area and Solar Radiation Interception by Orange Tree Top. *Bragantia* **2015**, *74* (4), 476–482. https://doi.org/10.1590/1678-

4499.0130.

(95) Gausman, H. W.; Allen, W. A. Optical Parameters of Leaves of 30 Plant Species. *Plant Physiol.* **1973**, *52*, 57–62. https://doi.org/10.1104/pp.52.1.57.

(96) Feng, G.; Luo, H.; Zhang, Y.; Gou, L.; Yao, Y.; Lin, Y.; Zhang, W. Relationship between Plant Canopy Characteristics and Photosynthetic Productivity in Diverse Cultivars of Cotton (Gossypium Hirsutum L.). *Crop J.* **2016**, *4*, 499–508. https://doi.org/10.1016/j.cj.2016.05.012.

(97) DeRose, R. J.; Seymour, R. S. Patterns of Leaf Area Index during Stand Development in Even-Aged Balsam Fir – Red Spruce Stands. *Can. J. For. Res.* **2010**, *40*, 629–637. https://doi.org/10.1139/x10-018.

(98) Peterson, J. S. *Plant Fact Sheet for Douglas Fir*; 2002.

(99) Gutiérrez-Rodríguez, M.; Escalante-Estrada, J. A.; Rodriguez Gonzalez, M. T.; Reynolds, M. P. Canopy Reflectance Indices and Its Relationship with Yield in Common Bean Plants (Phaseolus Vulgaris L.) with Phosphorous Supply. *Int. J. Agric. Biol.* **2006**, *8* (2), 203–207.

(100) Chakwizira, E.; Moot, D. J.; Scott, W. R.; Fletcher, A. L.; Maley, S. Leaf Development, Radiation Interception and Radiation-Use Efficiency of Kale Crops Supplied with Different Rates of Banded or Broadcast Phosphorus Fertiliser. *Crop Pasture Sci.* **2011**, *62*, 840–847. https://doi.org/10.1071/CP10359.

(101) Balkaya, A.; Yanmaz, R. Promising Kale (Brassica Oleracea Var. Acephala) Populations from Black Sea Region, Turkey. *New Zeal. J. Crop Hortic. Sci.* **2005**,

33, 1–7. https://doi.org/10.1080/01140671.2005.9514324.

(102) Slamet, W.; Purbajanti, E. D.; Darmawati, A.; Fuskhah, E. Leaf Area Index, Chlorophyll, Photosynthesis Rate of Lettuce (Lactuca Sativa L) under N-Organic Fertilizer. *Indian J. Anim. Res.* **2017**, *51* (4), 365–369. https://doi.org/10.18805/ijare.v51i04.8424.

(103) Lacerda, P.; Viana, P. M. F.; da Silva, G. C.; Teixeira, I. R. Geotextiles Influence on the Formation of Soil Wet Bulbs and the Production of Drip-Irrigated Lettuce. *Aust. J. Crop Sci.* **2016**, *10* (7), 1007–1014. https://doi.org/10.21475/ajcs.2016.10.07.p7691.

(104) Burton, A. J.; Pregitzer, K. S.; Reed, D. D. Leaf Area and Foliar Biomass Relationships in Northern Hardwood Forests Located along an 800 Km Acid Deposition Gradient. *For. Sci.* **1991**, *37* (4), 1041–1059.

(105) Gilman, E. F.; Watson, D. G. *Acer Rubrum, Red Maple*; 1993. https://doi.org/10.1017/cbo9781107252806.079.

(106) Coble, A. P.; Cavaleri, M. A. Vertical Leaf Mass per Area Gradient of Mature Sugar Maple Reflects Both Height-Driven Increases in Vascular Tissue and Light-Driven Increases in Palisade Layer Thickness. *Tree Physiol.* **2017**, *37* (10), 1337–1351. https://doi.org/10.1093/treephys/tpx016.

(107) Rossi, F.; Nerozzi, F.; Facini, O.; Georgiadis, T. Determination of Peach Leaf Area Index by Radiation Measurements. *J. Hortic. Sci.* **1995**, *70* (4), 683–689.

(108) Gilman, E. F.; Watson, D. G. *Prunus Persica Peach*; 1994.

(109) Kiniry, J. R.; Simpson, C. E.; Schubert, A. M.; Reed, J. D. Peanut Leaf Area Index, Light Interception, Radiation Use Efficiency, and Harvest Index at Three Sites in Texas. *F. Crop. Res.* **2005**, *91* (2–3), 297–306. https://doi.org/10.1016/j.fcr.2004.07.021.

(110) Sankar, B.; Gopinathan, P.; Karthishwaran, K.; Somasundaram, R. Leaf Anatomical Changes in Peanut Plants in Relation to Drought Stress with or without Paclobutrazol and Abscisic Acid. **2013**, 25–29.

(111) Urban, J.; Tatarinov, F.; Nadezhdina, N.; Čermák, J.; Ceulemans, R. Crown Structure and Leaf Area of the Understorey Species Prunus Serotina. *Trees - Struct. Funct.* **2009**, *23* (2), 391–399. https://doi.org/10.1007/s00468-008-0288-6.

(112) Gilman, E. F.; Watson, D. G. *Prunus Cerasifera 'Newportii' Newport Cherry Plum*; 1994.

(113) Bennett, J. P.; Rassat, P.; Berrang, P.; Karnosky, D. F. Relationships between Leaf Anatomy and Ozone Sensitivity of Fraxinus Pennsylvanica Marsh. and Prunus Serotina Ehrh. *Environ. Exp. Bot.* **1992**, *32* (1), 33–41. https://doi.org/10.1016/0098-8472(92)90027-Y.

(114) Tripathi, A. M.; Fischer, M.; Trnka, M.; Orság, M.; Vanbeveren, S. P. P.; Marek, M. V. Leaf Area Index Development and Radiation Use Efficiency of a Poplar Short Rotation Coppice Culture. In *Global Change: A Complex Challenge*; 2015; pp 1–5. https://doi.org/10.13140/RG.2.1.5118.4486.

(115) Gilman, E. F.; Watson, D. G. *Populus Alba: White Poplar*.

(116) Gordon, R.; Brown, D. M.; Dixon, M. A. Estimating Potato Leaf Area Index for Specific Cultivars. *Potato Res.* **1997**, *40* (3), 251–266. https://doi.org/10.1007/BF02358007.

(117) Wu, L.; Long, Y.; Sun, H.; Liu, N.; Wang, W.; Dong, Q. Length Measurement of Potato Leaf Using Depth Camera. *IFAC-PapersOnLine* **2018**, *51* (17), 314–320. https://doi.org/10.1016/j.ifacol.2018.08.197.

(118) Park, H. J.; Lee, A.; Lee, S. S.; An, D. J.; Moon, K. B.; Ahn, J. C.; Kim, H. S.; Cho, H. S. Overexpression of Golgi Protein CYP21-4s Improves Crop Productivity in Potato and Rice by Increasing the Abundance of Mannosidic Glycoproteins. *Front. Plant Sci.* **2017**, *8* (July), 1–13. https://doi.org/10.3389/fpls.2017.01250.

(119) Smither-Kopperl, M. *Plant Guide for Lacy Phacelia (Phacelia Tanacetifolia)*; Lockeford, CA 95237, 2018.

(120) Yeo, K. H.; Cho, Y. Y.; Lee, Y. B. Estimation of Growth and Yield for Single-Stemmed Rose “Vital” in a Single Stem System. *Hortic. Environ. Biotechnol.* **2011**, *52* (5), 455–465. https://doi.org/10.1007/s13580-011-0146-0.

(121) Rouphael, Y.; Mouneimne, A. H.; Ismail, A.; Mendoza-De Gyves, E.; Rivera, C. M.; Colla, G. Modeling Individual Leaf Area of Rose (Rosa Hybrida L.) Based on Leaf Length and Width Measurement. *Photosynthetica* **2010**, *48* (1), 9–15. https://doi.org/10.1007/s11099-010-0003-x.

(122) Machuca, A.; Palma, D.; Tapia, M. L.; Lizana, L. A.; Escalona, V. Planting Densities Affect Nitrate Concentration in Spinach (Spinacia Oleracea L.)

Cultivated in Floating Hydroponic System Root. In *2015 American Society for Horticultural Sciences Annual Meeting*; New Orleans, Louisiana, 2015.

(123) Spinach | Diseases and Pests, Description, Uses, Propagation https://plantvillage.psu.edu/topics/spinach/infos (accessed May 23, 2020).

(124) Boese, S. R.; Huner, N. P. A. Effect of Growth Temperature and Temperature Shifts on Spinach Leaf Morphology and Photosynthesis. *Plant Physiol.* **1990**, *94* (4), 1830–1836. https://doi.org/10.1104/pp.94.4.1830.

(125) *Colorado (Blue) Spruce*.

(126) Bélanger, G.; Richards, J. E. Growth Analysis of Timothy Cultivars Differing in Maturity. *Can. J. Plant Sci.* **1995**, *75*, 643–648. https://doi.org/10.4141/cjps95-109.

(127) Ogle, D. G.; St. John, L.; Tilley, D. J. *Plant Guide for Timothy (Phleum Pratense)*; Boise, Idaho, 2011.

(128) Garnier, E.; Laurent, G. Leaf Anatomy, Specific Mass and Water Content in Congeneric Annual and Perennial Grass. *Source New Phytol.* **1994**, *128* (4), 725–736.

(129) Arnó, J.; Del Moral, I.; Escolà, A.; Company, J.; Masip, J.; Sanz, R.; Rosell, J. R.; Martínez-Casasnovas, J. A. MAPPING THE LEAF AREA INDEX IN VINEYARD USING A GROUND-BASED LIDAR SCANNER J. Arnó, I. Del Moral, A. Escolà, J. Company, J. Masip, R. Sanz, and J.R. Rosell. *Conference* **2012**, No. July.

(130) Grape | Diseases and Pests, Description, Uses, Propagation https://plantvillage.psu.edu/topics/grape/infos (accessed May 23, 2020).

(131) Hagin, R. D.; Linscott, D. L.; Dawson, J. E. 2,4-d Metabolism in Resistant Grasses. *J. Agric. Food Chem.* **1970**, *18*, 848–850.

(132) Sundaram, K. M. S.; Sundaram, A.; Curry, J.; Sloane, L. Dissipation Kinetics of Azadirachtin in Some Forest Matrices and Its Systemic Translocation in Conifers for Spruce Budworm Control. *J. Environ. Sci. Heal. - Part B Pestic. Food Contam. Agric. Wastes* **1997**, *32* (5), 803–829. https://doi.org/10.1080/03601239709373114.

(133) Sarais, G.; Angioni, A.; Lai, F.; Cabras, P.; Caboni, P. Persistence of Two Neem Formulations on Peach Leaves and Fruit: Effect of the Distribution. *J. Agric. Food Chem.* **2009**, *57* (6), 2457–2461. https://doi.org/10.1021/jf803697h.

(134) Sundaram, K. M. S.; Sundaram, A.; Curry, J.; Sloane, L. Formulation Selection, and Investigation of Azadirachtin-A Persistence in Some Terrestrial and Aquatic Components of a Forest Environment. *Pestic. Sci.* **1997**, *51* (1), 74–90. https://doi.org/10.1002/(SICI)1096-9063(199709)51:1<74::AID-PS606>3.0.CO;2-J.

(135) Antonious, G. F.; Turley, E. T.; Abubakari, M.; Snyder, J. C. Dissipation, Half-Lives, and Mass Spectrometric Identification of Chlorpyrifos and Its Two Metabolites on Field-Grown Collard and Kale. *J. Environ. Sci. Heal. - Part B Pestic. Food Contam. Agric. Wastes* **2017**, *52* (4), 251–255. https://doi.org/10.1080/03601234.2016.1270683.

(136) Ware, G. W.; Estesen, B. J.; Buck, N. A. Dislodgable Insecticide Residues on Cotton. *Bull. Environ. Contam. Toxicol.* **1978**, *20*, 24–27.

(137) Buck, N. A.; Estesen, B. J.; Ware, G. W. Dislodgable Insecticide Residues on Cotton Foliage: Fenvalarate, Permethrin, Sulprofos, Chlorpyrifos, Methyl Parathion, EPN, Oxamyl, and Profenofos. *Bull. Environ. Contam. Toxicol.* **1980**, *24*, 283–288.

(138) Ware, G. W.; Buck, N. A.; Estesen, B. J. Dislodgeable Insecticide Residues on Cotton Foliage: Comparison of ULV/Cottonseed Oil vs. Aqueous Dilutions of 12 Insecticides. *Bull. Environ. Contam. Toxicol.* **1983**, *31* (5), 551–558.

(139) Montemurro, N.; Grieco, F.; Lacertosa, G.; Visconti, A. Chlorpyrifos Decline Curves and Residue Levels from Different Commercial Formulations Applied to Oranges. *J. Agric. Food Chem.* **2002**, *50* (21), 5975–5980. https://doi.org/10.1021/jf0256687.

(140) Kumar, A.; Nadda, G.; Shanker, A. Determination of Chlorpyrifos 20% EC (Dursban 20 EC) in Scented Rose and Its Products. *J. Chromatogr. A* **2004**, *1050*, 193–199. https://doi.org/10.1016/j.chroma.2004.08.050.

(141) Chang-Yen, I.; Nickless, G.; Pickard, J. A. Effect of Pesticide Formulation on the Distribution of Fenitrothion on Apple Foliage. *J. Agric. Food Chem.* **1983**, *31*, 1137–1139.

(142) LaPierre, L. E. Persistence of Fenitrothion Insecticide in Poplar Populus Tremuloides and Gray Birch Betula Populifolia. *Bull. Environ. Contam. Toxicol.* **1985**, *35*, 471–475.

(143) Yule, W. N.; Duffy, J. R. The Persistence and Fate of Fenitrothion Insecticide. *Bull. Environ. Contam. Toxicol.* **1972**, *8* (1), 10–18.

(144) Malhat, F. M. Residues and Dissipation of Fenitrothion in Green Bean (Phaseolus Vulgaris) and Soil. *Soil Sci.* **2012**, *2012*, 1–4. https://doi.org/10.5402/2012/365317.

(145) Yule, W. N.; Varty, I. W. The Persistence and Fate of Fenitrothion Insecticide in a Forest Environment. III. Deposit and Residue Studies with Black Spruce and Red Maple. *Bull. Environ. Contam. Toxicol.* **1975**, *13* (678–680).

(146) Sundaram, K. M. S. A Comparative Evaluation of Dislodgable and Penetrated Residues, and Persistence Characteristics of Aminocarb and Fenitrothion, Following Application of Several Formulation onto Conifer Trees. *J. Environ. Sci. Heal.* **1986**, *21* (6), 539–560.

(147) Likas, D. T.; Tsiropoulos, N. G. Behaviour of Fenitrothion Residues in Leaves and Soil of Vineyard after Treatment with Microencapsulate and Emulsified Formulations. *Int. J. Environ. Anal. Chem.* **2007**, *87* (13–14), 927–935. https://doi.org/10.1080/03067310701409317.

(148) Draper, W. M.; Street, J. C. Drift from a Commercial, Aerial Application of Methyl and Ethyl Parathion: An Estimation of Potential Human Exposure. *Bull. Environ. Contam. Toxicol.* **1981**, *26*, 530–536.

(149) Fahey, J. E.; Hamilton, D. W.; Rings, R. W. Longevity of Parathion and Related Insecticides in Spray Residues. *J. Econ. Entomol.* **1952**, *45*, 700–703.

(150) Attri, B. S.; Lal, R. Residues and Residual Toxicity of Ethyl and Methyl Parathion

on Cauliflower. *Indian J. Agric. Sci.* **1974**, *44* (6), 361–365.

(151) Thompson, N. P.; Brooks, R. F. Disappearance of Dislodgable Residues of Five Organophosphate Pesticides on Citrus Leaves and Fruit during Dry and Wet Weather in Florida. *Arch. Environ. Contam. Toxicol.* **1976**, *5*, 55–61.

(152) Ware, G. W.; Estesen, B. J.; Cahill, W. P. Organophosphate Residues on Cotton in Arizona. *Bull. Environ. Contam. Toxicol.* **1972**, *8*, 361–362.

(153) Ware, G. W.; Estesen, B. J.; Cahill, W. P. Dislodgable Leaf Residues of Insecticide on Cotton. *Bull. Environ. Contam. Toxicol.* **1974**, *11*, 434–437.

(154) Cahill, W. P.; Estesen, B. J.; Ware, G. W. Foliage Residues of Insecticides on Cotton. *Bull. Environ. Contam. Toxicol.* **1975**, *13*, 334–337.

(155) McDowell, L. L.; Willis, G. H.; Southwick, L. M.; Smith Jr., S. Interception and Persistence of Parathion and Fenvalerate on Cotton Plants as a Function of Application Method. *Pestic. Sci.* **1991**, *33* (3), 271–279.

(156) Archer, T. E. Dissipation of Parathion and Related Compounds from Field-Sprayed Lettuce. *J. Agric. Food Chem.* **1975**, *23* (5), 858–860.

(157) Winterlin, W.; Bailey, J. B.; Langbehn, L.; Mourer, C. Degradation of Parathion Applied to Peach Leaves. *Pestic. Monit. J.* **1975**, *8* (4), 263–269.

(158) Staiff, D. C.; Davis, J. E.; Robbins, A. L. Parathion Residues on Apple and Peach Foliage as Affected by the Presence of Fungicides, Maneb and Zineb. *Bull. Environ. Contam. Toxicol.* **1977**, *17* (3), 293–301.

(159) Woodrow, J. E.; Seiber, J. N.; Crosby, D. G.; Moilanen, K. W.; Soderquist, C. J.;

Mourer, C. Airborne and Surface Residues of Parathion and Its Conversion Products in a Treated Plum Orchard Environment. *Arch* **1977**, *6*, 175–191.

(160) Archer, T. E. Dissipation of Parathion and Related Compounds from Field-Sprayed Spinach. *J. Agric. Food Chem.* **1974**, *22*, 974–977.

(161) Anderson, J.; West Jennifer. Global cloud cover | Eclipsophile http://eclipsophile.com/global-cloud-cover/ (accessed Feb 26, 2019).

(162) Thorsen, S. timeanddate.com https://www.timeanddate.com/ (accessed Feb 14, 2019).

(163) Rüdel, H. Volatilisation of Pesticides from Soil and Plant Surfaces. *Chemosphere* **1997**, *35* (1–2), 143–152. https://doi.org/10.1016/S0045-6535(97)00146-X.

(164) Tsialtas, J. T.; Maslaris, N. Leaf Shape and Its Relationship with Leaf Area Index in a Sugar Beet (Beta Vulgaris L.) Cultivar. *Photosynthetica* **2007**, *45* (4), 527–532. https://doi.org/10.1007/s11099-007-0090-5.

(165) Luković, J.; Maksimović, I.; Zorić, L.; Nagl, N.; Perčić, M.; Polić, D.; Putnik-Delić, M. Histological Characteristics of Sugar Beet Leaves Potentially Linked to Drought Tolerance. *Ind. Crops Prod.* **2009**, *30* (2), 281–286. https://doi.org/10.1016/j.indcrop.2009.05.004.

APPENDIX

LIST OF TABLES

Page

LIST OF FIGURES

LIST OF SECTIONS

Table A1. Pesticide physicochemical input parameters

Pesticide	$k_{photo,ref}$ (h^{-1})	Ref.	I_{ref} ($W\ m^{-2}$)	Ref.	Log $K_{octanol-water}$[a]	Log $K_{air-water}$[a]	Vapor Pressure[a] (Pa at 25°C)
2,4-D	2.90×10^{-2}	47	320	47	2.81	-5.839	1.52×10^{-1}
Azadirachtin	4.33×10^{-2}	48	500	48	1.09	-11.395	3.08×10^{-3}
Chlorothalonil	2.71×10^{-3}	49	500	49	3.66	-4.087	1.27×10^{-2}
Chlorpyrifos	1.37×10^{-3}	29	1000	29	4.96	-3.922	3.99×10^{-3}
Fenitrothion	1.11×10^{-2}	50	500	50	3.30	-4.420	7.20×10^{-3}
Indoxacarb	3.70×10^{-2}	*b*	550	*b*	4.60	-10.954	1.17×10^{-10}
Lambda-cyhalothrin	5.50×10^{-2}	*b*	550	*b*	7.00	-4.218	1.50×10^{-9}
Parathion	2.22×10^{-2}	50	500	50	3.83	-4.914	8.91×10^{-4}

[a]indicates value was obtained from EPI Suite[79]; [b]indicates value was obtained from experiments described in chapter 3.

Table A2. Input parameters for Bird's Clear Sky Model

Input	Value
Ozone thickness (cm)	0.4
Water vapor thickness (cm)	6.5
Aerosol optical depth @ 500 nm	0.5
Aerosol optical depth @ 380 nm	0.5
Forward scattering	0.85
Albedo	0.25

Table A3. Plant input parameters for plants used in PeDAL model evaluation

Plant	Leaf Area Index[a]	Ref.	Leaf length[b] (m)	Ref.	Leaf thickness[b] (m)	Ref.
Alfalfa	6.1	[80]	0.02	Measured[c]	0.000150	[81]
Apple	6.0	[82]	0.06	[83]	0.000150	[84]
Aspen	2.3	[85]	0.08	[86]	0.000173	(A)[d]
Birch	2.7	[87]	0.08	[88]	0.000173	[89]
Cauliflower	5.0	[90]	0.20	(B)[d]	0.000200	(B)[d]
Chinese cabbage	2.8	[91]	0.20	[92]	0.000200	[93]
Citrus/Orange	4.3	[94]	0.10	[81]	0.000245	[95]
Collards	5.0	(C)[d]	0.20	(C)[d]	0.000300	(C)[d]
Cotton	5.0	[96]	0.11	[83]	0.000209	[95]
Fir	19.2	[97]	0.03	[98]	0.001600	[98]
Green bean	5.5	[99]	0.10	[83]	0.000263	[95]
Kale	5.0	[100]	0.20	[101]	0.000300	[101]
Lettuce	4.7	[102]	0.12	[103]	0.000720	[95]
Maple	9.2	[104]	0.10	[105]	0.000175	[106]
Peach	14.0	[107]	0.15	[108]	0.000152	[95]
Peanut	8.5	[109]	0.03	[83]	0.000215	[110]
Plum	5.0	[111]	0.08	[112]	0.000200	[113]
Poplar	7.3	[114]	0.15	[115]	0.000173	(A)[d]
Potato	2.0	[116]	0.03	[117]	0.000225	[118]
Purple tansy	6.1	(D)[d]	0.02	[119]	0.000150	(D)[d]
Rose	5.0	[120]	0.10	[121]	0.000150	[95]
Spinach	5.0	[122]	0.15	[123]	0.000400	[124]
Spruce	25.2	[97]	0.03	[125]	0.001600	[125]
Timothy grass	11	[126]	0.25	[127]	0.000175	[128]
Vineyard	2.1	[129]	0.15	[130]	0.000215	(E)[d]

[a] *If a single value was reported, that value was used. If a range of values were given, the maximum value is shown here.*

[b] *If a single value was reported, that value was used. If a range of values were given, the average value is shown here.*

[c] *"Measured" indicates that we obtained the value by measuring the leaf length of 15 leaves collected from a plot near Logan, Utah; the average is reported.*

[d] *When values were not available in the literature, we used measurements reported for similar plants. "A" indicates the value for birch was used. "B" indicates the value for Chinese cabbage was used. "C" indicates the value for kale was used. "D" indicates the value for alfalfa was used. "E" indicates the value for peanut was used.*

Table A4. Application input parameters for scenarios used in PeDAL model evaluation

Scenario	Ref.	Date of Application	Spray time[a]	Latitude (North is positive)	Longitude (East is positive)	Elevation (m)	Time Zone	Field Area (m^2)[b]	Mass of a.i. applied (g)[c]
2,4-D on timothy grass	[131]	June 15	12:00 PM	42.44°	-76.50°	123	-5	36	8
Azadirachtin on aspen	[132]	June 26	8:00 AM	46.38°	-84.02°	192	-5	10000	100
Azadirachtin on peach	[133]	August 15	12:00 PM	39.36°	9.00°	58	+1	10000	188
Azadirachtin on spruce	[134]	June 13	9:00 AM	46.38°	-84.02°	192	-5	10000	60
Azadirachtin on spruce	[132]	June 26	8:00 AM	46.38°	-84.02°	192	-5	10000	100
Chlorothalonil on Chinese cabbage	[68]	October 27	12:00 PM	33.14°	119.79°	45	+8	45	6
Chlorothalonil on peanut	[67]	August 3	12:00 PM	31.45°	-83.51°	108	-5	10000	1260
Chlorpyrifos on	[68]	October 27	12:00 PM	33.14°	119.79°	45	+8	45	6

Chinese cabbage									
Chlorpyrifos on collards	[135]	August 1	12:00 PM	38.20°	-84.87°	155	-5	81	9
Chlorpyrifos on cotton	[136]	August 9	12:00 PM	32.44°	-111.22°	607	-7	62	7
Chlorpyrifos on cotton	[137]	July 17	12:00 PM	32.44°	-111.22°	607	-7	124	34
Chlorpyrifos on cotton	[138]	July 12	12:00 PM	32.44°	-111.22°	607	-7	124	34
Chlorpyrifos on kale	[135]	August 1	12:00 PM	38.20°	-84.87°	155	-5	81	9
Chlorpyrifos on orange	[139]	October 27	12:00 PM	40.39°	16.72°	26	+1	1200	84
Chlorpyrifos on potato	[40]	June 25	12:00 PM	52.85°	4.97°	-3	+1	10000	679
Chlorpyrifos on purple tansy	[69]	January 8	8:00 AM	-45.23°	-160.70°	500	+12	12600	200
Chlorpyrifos on rose	[140]	May 15	7:00 AM	32.11°	76.54°	1472	+5	10000	100

Fenitrothion on apple	[141]	April 1	12:00 PM	51.45°	-2.59°	11	0	10000	230
Fenitrothion on apple	[141]	April 23	12:00 PM	51.45°	-2.59°	11	0	10000	110
Fenitrothion on apple	[141]	April 23	12:00 PM	51.45°	-2.59°	11	0	10000	230
Fenitrothion on apple	[141]	May 1	12:00 PM	51.45°	-2.59°	11	0	10000	90
Fenitrothion on apple	[141]	May 4	12:00 PM	51.45°	-2.59°	11	0	10000	60
Fenitrothion on birch	[142]	May 26	12:00 PM	46.33°	-65.50°	19	-4	10	0.5
Fenitrothion on birch	[142]	June 5	12:00 PM	46.33°	-65.50°	19	-4	10	0.5
Fenitrothion on fir	[143]	June 14	12:00 PM	46.52°	-66.29°	19	-4	4047000	114000
Fenitrothion on green bean	[144]	May 11	12:00 PM	30.46°	30.94°	229	+2	40	5

Fenitrothion on maple	[145]	May 30	12:00 PM	45.96°	-66.64°	17	-4	4047	86
Fenitrothion on poplar	[142]	May 26	12:00 PM	46.33°	-65.50°	19	-4	10	0.5
Fenitrothion on poplar	[142]	June 5	12:00 PM	46.33°	-65.50°	19	-4	10	0.5
Fenitrothion on spruce	[145]	May 30	12:00 PM	45.96°	-66.64°	17	-4	4047	86
Fenitrothion on spruce	[143]	June 14	12:00 PM	46.52°	-66.29°	19	-4	4047000	114000
Fenitrothion on spruce	[146]	May 13	12:00 PM	45.60°	-76.50°	167	-5	1000	34
Fenitrothion on vineyard	[147]	August 28	12:00 PM	39.28°	22.82°	3	+2	186	14
Parathion on alfalfa	[148]	July 2	8:00 AM	40.46°	-109.53°	1624	-7	295420	4139
Parathion on apple	[149]	June 6	12:00 PM	40.81°	-81.94°	304	-5	10000	100
Parathion on cauliflower	[150]	February 1	12:00 PM	28.61°	77.21°	216	+5	38.5	2

Parathion on citrus	[151]	April 5	12:00 PM	28.09°	-81.72°	53	-5	10000	100
Parathion on citrus	[151]	June 4	12:00 PM	28.09°	-81.72°	53	-5	10000	100
Parathion on cotton	[152]	July 12	12:00 PM	32.44°	-111.52°	607	-7	231	26
Parathion on cotton	[153]	July 10	12:00 PM	32.88°	-111.52°	450	-7	4047	453
Parathion on cotton	[154]	August 6	12:00 PM	32.88°	-111.52°	450	-7	4047	453
Parathion on cotton	[155]	July 28	12:00 PM	34.37°	-89.52°	154	-6	100000	2800
Parathion on lettuce	[156]	June 15	12:00 PM	38.54°	-121.74°	16	-8	4047	340
Parathion on peach	[157]	July 10	12:00 PM	37.66°	-120.99°	27	-8	80937	9071
Parathion on peach	[157]	August 3	12:00 PM	37.66°	-120.99°	27	-8	80937	18142

Parathion on peach	[158]	August 14	12:00 PM	47.42°	-120.31°	237	-8	10000	100
Parathion on plum	[159]	August 21	12:00 PM	36.61°	-119.53°	105	-8	3200	704
Parathion on potato	[55]	August 18	1:00 PM	52.53°	5.60°	-3	+1	24960	2496
Parathion on spinach	[160]	June 15	12:00 PM	38.54°	-121.74°	16	-8	4047	340

[a]12:00pm was used as the default spray time unless an actual spray time was specified in the literature. [b]A default field area of 10,000 m^2 was used as the default unless dimensions were specified in the literature. [c]A default mass of 100 grams was used for the mass of active ingredient applied unless more specific application information was specified in the literature

Table A5. Meteorological input parameters for scenarios used in PeDAL model evaluation

Scenario	Ref.	Study Location	Temp. (°C)[a]	Wind Speed (m/s)[b]	Cloud Coverage (%)[c]	Relative Humidity (%)	Timeanddate.com location used
2,4-D on timothy grass	[131]	Ithaca, NY	26.4	3.1[z]	60	71[z]	Binghamton Regional Airport
Azadirachtin on aspen	[132]	Laird Township, Ontario, Canada	24[z]	2.7[z]	55	73[z]	Sault Ste. Marie
Azadirachtin on peach	[133]	San Sperate, Italy	28.9[z]	4.0[z]	25	68[z]	Cagliari/Elmas
Azadirachtin on spruce	[134]	Laird Township, Ontario, Canada	23.2	2.7[z]	55	80	Sault Ste. Marie
Azadirachtin on spruce	[132]	Laird Township, Ontario, Canada	24[z]	2.7[z]	55	73[z]	Sault Ste. Marie
Chlorothalonil on Chinese cabbage	[68]	Jiangsu, China	21.3	2.2[z]	35	74[z]	Nanjing
Chlorothalonil on peanut	[67]	Tifton, GA	30.8	1.8[z]	50	76[z]	Valdosta Regional Airport
Chlorpyrifos on Chinese cabbage	[68]	Jiangsu, China	21.3	2.2[z]	35	74[z]	Nanjing
Chlorpyrifos on collards	[135]	Frankfort, KY	28[z]	1.8[z]	45	66	Frankfort
Chlorpyrifos on cotton	[136]	Marana, AZ	33.5	3.1[z]	20	46[z]	Davis-Monthan Air Force Base
Chlorpyrifos on cotton	[137]	Marana, AZ	34.4	3.6[z]	25	40[z]	Davis-Monthan Air Force Base

Chlorpyrifos on cotton	[138]	Marana, AZ	35.5	3.6[z]	25	40[z]	Davis-Monthan Air Force Base
Chlorpyrifos on kale	[135]	Frankfort, KY	28[z]	1.8[z]	45	66	Frankfort
Chlorpyrifos on orange	[139]	Metaponto, Italy	21.6	1.6	40	66	n/a
Chlorpyrifos on potato	[40]	Slootdorp, Netherlands	20.3	3.0	70	77[z]	Amsterdam Schipol Airport
Chlorpyrifos on purple tansy	[69]	Ida Valley, New Zealand	18.9	5.3	55	58	n/a
Chlorpyrifos on rose	[140]	Palampur, India	27.3	2.2[z]	60	27	Lucknow/Amausi
Fenitrothion on apple	[141]	Bristol, England	11.7[z]	4.9[z]	60	74[z]	Filton Private
Fenitrothion on apple	[141]	Bristol, England	11.7[z]	4.9[z]	60	74[z]	Filton Private
Fenitrothion on apple	[141]	Bristol, England	11.7[z]	4.9[z]	60	74[z]	Filton Private
Fenitrothion on apple	[141]	Bristol, England	14.2[z]	4.9[z]	70	74[z]	Filton Private
Fenitrothion on apple	[141]	Bristol, England	14.2[z]	4.9[z]	70	74[z]	Filton Private
Fenitrothion on birch	[142]	Moncton, N.B., Canada	13.1[z]	4.5[z]	50	73[z]	Moncton
Fenitrothion on birch	[142]	Moncton, N.B., Canada	18.1[z]	4.0[z]	50	76[z]	Moncton
Fenitrothion on fir	[143]	Priceville, N.B., Canada	19.4[z]	3.1[z]	60	72[z]	Fredericton
Fenitrothion on green bean	[144]	El Menofiya, Egypt	25	4.0[z]	10	49[z]	Cairo Airport
Fenitrothion on maple	[145]	Fredericton, N.B., Canada	19.4[z]	3.1[z]	60	72[z]	Fredericton
Fenitrothion on poplar	[142]	Moncton, N.B., Canada	13.1[z]	4.5[z]	50	73[z]	Moncton
Fenitrothion on poplar	[142]	Moncton, N.B., Canada	18.1[z]	4.0[z]	50	76[z]	Moncton

Fenitrothion on spruce	[145]	Fredericton, N.B., Canada	19.4[z]	3.1[z]	60	72[z]	Fredericton
Fenitrothion on spruce	[143]	Priceville, N.B., Canada	19.4[z]	3.1[z]	60	72[z]	Fredericton
Fenitrothion on spruce	[146]	Shawville, Quebec, Canada	15.6[z]	2.7[z]	60	67[z]	Petawawa
Fenitrothion on vineyard	[147]	Nea Aghialos, Greece	22.7[z]	2.7[z]	15	66	Skiathos Island
Parathion on alfalfa	[148]	Vernal, UT	24.7[z]	3.1[z]	35	33[z]	Rock Springs
Parathion on apple	[149]	Wooster, OH	23.1[z]	2.7[z]	55	72[z]	Wayne County Airport
Parathion on cauliflower	[150]	New Delhi, India	20.5	1.8[z]	25	66[z]	New Delhi
Parathion on citrus	[151]	Lake Alfred, FL	25.6[z]	3.1[z]	45	62[z]	Lakeland Regional
Parathion on citrus	[151]	Lake Alfred, FL	30[z]	2.2[z]	50	71[z]	Lakeland Regional
Parathion on cotton	[152]	Marana, AZ	34	3.6[z]	25	57	Davis-Monthan Air Force Base
Parathion on cotton	[153]	La Palma, AZ	36.8	1.8[z]	25	28[z]	Phoenix Sky Harbor International Airport
Parathion on cotton	[154]	La Palma, AZ	35.8	1.8[z]	20	32[z]	Phoenix Sky Harbor International Airport
Parathion on cotton	[155]	Oxford, MS	30.6[z]	2.7[z]	45	72[z]	Oxford
Parathion on lettuce	[156]	Davis, CA	27.2[z]	3.6[z]	10	50[z]	Sacramento International Airport
Parathion on peach	[157]	Modesto, CA	30.3[z]	3.6[z]	15	40[z]	Modesto
Parathion on peach	[157]	Modesto, CA	29.5[z]	3.1[z]	10	42[z]	Modesto
Parathion on peach	[158]	Wenatchee, WA	26.9[z]	3.6[z]	45	40[z]	Pangborn Memorial Airport

Parathion on plum	[159]	Parlier, CA	30.3[z]	1.8[z]	10	51[z]	Visalia Municipal
Parathion on potato	[55]	Biddinghuizen, Netherlands	20.0	2.0	60	79[z]	Amsterdam Schipol Airport
Parathion on spinach	[160]	Davis, CA	27.2[z]	3.6[z]	10	50[z]	Sacramento International Airport

Any input parameter without a superscript next to it was taken directly from the literature source.

[a] *Information about the time and height at which temperatures were measured were not provided in the literature sources. Temperatures shown here were calculated with equation 5 from them main manuscript.*

[b] *Information about the time and height at which wind speeds were measured were not provided in the literature sources. Wind speeds shown here are the average of values reported in literature sources.*

[c]*All input parameters for cloud coverage were estimated with data provided by eclipsophile.com.*[161]

[z] *Indicates the input parameter was estimated using the climate data section from timeanddate.com*[162] *for the nearest location to the spray site, which is listed in the rightmost column.*

Section A1. Selection of literature sources and determination of measured field DT_{50} values used in PeDAL model evaluation

For inclusion in model evaluation, we only used studies from the literature that met the following criteria:

1. Measured pesticide concentration was determined on leaves (not fruits, roots, other parts of the plant, the plant as a whole, or soil).
2. Application occurred in the field rather than a greenhouse.
3. Studies took place when there was no rainfall (exceptions for this were made if the rainfall was of limited quantity and/or occurred late enough after application that its impact on DT_{50} was deemed negligible). This was done because the PeDAL model does not currently model wash-off caused by precipitation.
4. Timing and location of study was clearly specified. Ideally, exact day and location of application was provided, but month and general location were needed at a minimum.
5. Dissipation study used an active ingredient that had a reported foliar photodegradation rate available in the literature.
6. An accurate DT_{50} value could determined from the information in the literature using the method outlined below.

DT_{50} values were recalculated according to the suggestions made by the Forum for Co-ordination of Pesticide Fate Models and their Use (FOCUS) to ensure their accuracy.[76] The only modification we made to the suggestions of FOCUS was to reduce the required number of data points to three to expand the number of studies included in the evaluation of the PeDAL model.

Reported residual concentrations were used for determining measured field DT_{50} values when they were available. In the case that penetrated and dislodgeable residues were reported separately, these values were summed to represent the total amount of pesticide remaining. In cases in which specific values weren't reported, graphs included in the literature were used to estimate concentrations. Initially all available values were used and data was then fit with a curve using equation A1:

$$c_{\mathrm{i,t}} = c_{\mathrm{i,o}} e^{-k_{\mathrm{diss}} t} \qquad \text{(A1)}$$

where t is the time since pesticide application, $c_{\mathrm{i,t}}$ is the concentration of pesticide *i* at time *t* after application, $c_{\mathrm{i,o}}$ is the original concentration of pesticide *i* immediately following application, and k_{diss} is the first-order dissipation rate constant, which incorporates all dissipation processes.

According to the suggestions of FOCUS, clear outliers or data points in the "lag phase" were eliminated to improve the fit of the curve and improve the accuracy of the DT_{50}.[76]

DT_{50}, which is analogous to the first half-life ($t_{1/2}$), was then calculated according to equation A2:

$$DT_{50}=t_{1/2}=\frac{0.693}{k_{diss}} \quad \text{(A2)}$$

In cases in which the effects of different formulations on a.i. dissipation were studied, each formulation had its DT_{50} calculated individually. The DT_{50} values for all formulations were then averaged and this average DT_{50} was used as a representative value for evaluation purposes. However, if different formulations were applied on different days then each of those scenarios were treated as individual data points in model evaluation.

Table A6. Input parameters used to produce data for chemical space diagrams

Parameter	Input for Figure 5 (and A2)	Input for Figure A2
Month	June	March
Day	20	20
Temperature (°C)	27	10
Wind speed (m/s)	2	2
Cloud coverage (%)	25	25
Relative humidity (%)	100	100
Latitude	41.76°N	41.76°N
Longitude	111.81°W	111.81°W
Time zone (Coordinated Universal Time)	-7	-7
Elevation (m)	1412	1412
Field area (m^2)	10000	10000
Spray time (24-h clock)	12	12
Mass applied (g)	100	100
%I	100	100
LAI	4.0	4.0
Leaf length (m)	0.10	0.10
Leaf thickness (m)	0.0002	0.0002

Chemical space diagrams were produced using R Studio Version 1.1.456. Simulations were run for >3000 hypothetical chemicals using the two sets of conditions shown in Table A6. Each set of simulations was repeated three times using different sets of input parameters for I_{ref} and $k_{photo(ref)}$. The I_{ref} and $k_{photo(ref)}$ values listed in Table A1 for chlorpyrifos, parathion, and 2,4-D were used to represent slow, moderate, and fast photodegradation, respectively.

Table A7. Input parameters for photodegradation sensitivity analysis

Location	Latitude	Longitude	Elevation (m)
Quito, Ecuador	0.18°S	78.47°W	2850
Fairbanks, Alaska	64.84°N	147.72°W	136
Orlando, FL	28.54°N	81.38°W	25
Logan, UT	41.76°N	111.81°W	1412
Duluth, MN	46.79°N	92.10°W	214

For these simulations, the plant properties of clover were used. Parathion's photodegradation rate in these simulations was based on the rate in Table A1; however, the log $K_{\text{octanol-water}}$ and log $K_{\text{air-water}}$ were set to 14 and -14, respectively. This was done to eliminate volatilization so that photodegradation could be examined alone. Default values were used for all other input parameters.

Table A8.1. Input parameters for typical spring and summer application conditions in Logan, Utah, USA

Parameter	Spring	Summer
Month	March	June
Day of Month	20	20
Wind speed (m/s)	1.6	1.1
Cloud coverage (%)	25	10
Relative Humidity (%)	30	50
Latitude	41.74	41.74
Longitude	-111.83	-111.83
Time Zone (Coordinated Universal Time)	-7	-7
Elevation (m)	1412	1412
Field area (m^2)	10000	10000
spray time (24-h clock)	6, 12, or 18	6, 12, or 18
Mass applied (g)	100	100
%I	100	100
$K_{\text{plant-air}}$ equation	generic	generic
LAI	4	4
leaf length (m)	0.1	0.1
leaf thickness (m)	0.0002	0.0002

The modeled DT_{50} value with constant photodegradation was obtained by overriding the BCSM intensity predictions and setting it at a constant intensity[25,27,34] of 500 W m^{-2}, which resulted in a constant photodegradation rate[50] of 2.22 x 10^{-2} h^{-1} .

Table A8.2. Hourly temperatures used for simulating typical spring and summer application conditions in Logan, Utah, USA

Time (24-h clock)	Spring temperature (°C)	Summer temperature (°C)
0	3.4	18.0
1	3.1	17.0
2	2.5	15.7
3	2.1	14.9
4	1.7	14.7
5	1.1	14.2
6	0.8	14.7
7	1.2	17.1
8	2.4	19.0
9	3.5	20.8
10	4.8	22.7
11	6.4	24.6
12	7.5	26.0
13	8.4	27.1
14	8.8	28.1
15	8.9	28.7
16	8.8	29.2
17	8.5	29.3
18	7.8	28.6
19	6.5	26.7
20	5.4	23.7
21	4.6	21.4
22	1.2	20.0
23	2.5	19.0

Table A9. Input parameters for generating emission flux values

Parameter	Parathion study[55]	Chlorpyrifos study[40]
Month	August	June
Day	18	25
Temperature (°C)	20	20.3
Wind speed (m/s)	2	3
Cloud coverage (%)	60	70
Relative humidity (%)	79	77
Latitude	52.53°N	52.85°N
Longitude	5.60°E	4.97°E
Time zone (Coordinated Universal Time)	+1	+1
Elevation (m)	-3	-3
Field area (m^2)	24960	10000
Spray time (24-h clock)	13	12
Mass applied (g)	2496	679
%I	80	80
LAI	2	2
Leaf length (m)	0.03	0.03
Leaf thickness (m)	0.000225	0.000225

All inputs match those used for model evaluation except for %I based on the IUPAC's technical report on plant interception of pesticide.[42] *Not doing so would have lead to an artificially high emission flux since volatilization occurs more readily from vegetation than soil.*[56,163]

Table A10. Measured and modeled DT_{50} values used in PeDAL model evaluation

	Pesticide	Plant	Location	Ref.	Measured DT_{50}	PeDAL DT_{50}
1	2,4-D	Timothy grass	Ithaca, NY	[131]	1.29	1.13
2	Azadirachtin	Aspen	Laird Township, Ontario, Canada	[132]	0.85	1.36
3	Azadirachtin	Peach	San Sperate, Italy	[133]	1.69	1.79
4	Azadirachtin	Spruce	Laird Township, Ontario, Canada	[134]	1.39	1.34
5	Azadirachtin	Spruce	Laird Township, Ontario, Canada	[132]	1.20	1.34
6	Chlorothalonil	Chinese cabbage	Jiangsu, China	[68]	3.63	0.60
7	Chlorothalonil	Peanut	Tifton, GA	[67]	2.78	0.27
8	Chlorpyrifos	Chinese cabbage	Jiangsu, China	[68]	4.71	4.94
9	Chlorpyrifos	Collards	Frankfort, KY	[135]	4.62	5.18
10	Chlorpyrifos	Cotton	Marana, AZ	[136]	0.47	0.81
11	Chlorpyrifos	Cotton	Marana, AZ	[137]	0.35	0.66
12	Chlorpyrifos	Cotton	Marana, AZ	[138]	0.51	0.55
13	Chlorpyrifos	Kale	Frankfort, KY	[135]	3.09	5.18
14	Chlorpyrifos	Orange	Metaponto, Italy	[139]	6.65	8.03
15	Chlorpyrifos	Potato	Slootdorp, Netherlands	[40]	0.39	1.37
16	Chlorpyrifos	Purple tansy	Ida Valley, New Zealand	[69]	0.63	2.21
17	Chlorpyrifos	Rose	Palampur, India	[140]	2.99	1.70
18	Fenitrothion	Apple	Bristol, England	[141]	0.66	1.01
19	Fenitrothion	Apple	Bristol, England	[141]	0.83	1.01
20	Fenitrothion	Apple	Bristol, England	[141]	0.70	1.01
21	Fenitrothion	Apple	Bristol, England	[141]	0.98	0.77
22	Fenitrothion	Apple	Bristol, England	[141]	1.63	0.76
23	Fenitrothion	Birch	Moncton, N.B., Canada	[142]	1.28	0.53
24	Fenitrothion	Birch	Moncton, N.B., Canada	[142]	1.79	0.29
25	Fenitrothion	Fir	Priceville, N.B., Canada	[143]	4.47	5.13
26	Fenitrothion	Green bean	El Menofiya, Egypt	[144]	0.99	0.46
27	Fenitrothion	Maple	Fredericton, N.B., Canada	[145]	1.29	1.08
28	Fenitrothion	Poplar	Moncton, N.B., Canada	[142]	2.19	1.77
29	Fenitrothion	Poplar	Moncton, N.B., Canada	[142]	2.03	1.06
30	Fenitrothion	Spruce	Fredericton, N.B., Canada	[145]	5.57	5.96

31	Fenitrothion	Spruce	Priceville, N.B., Canada	[143]	6.13	5.91
32	Fenitrothion	Spruce	Shawville, Quebec, Canada	[146]	8.53	7.12
33	Fenitrothion	Vineyard	Nea Aghialos, Greece	[147]	2.59	0.27
34	Parathion	Alfalfa	Vernal, UT	[148]	0.86	0.60
35	Parathion	Apple	Wooster, OH	[149]	0.96	1.21
36	Parathion	Cauliflower	New Delhi, India	[150]	1.97	3.13
37	Parathion	Citrus	Lake Alfred, FL	[151]	0.70	1.21
38	Parathion	Citrus	Lake Alfred, FL	[151]	0.85	0.96
39	Parathion	Cotton	Marana, AZ	[152]	0.41	0.44
40	Parathion	Cotton	La Palma, AZ	[153]	0.47	0.42
41	Parathion	Cotton	La Palma, AZ	[154]	0.58	0.49
42	Parathion	Cotton	Oxford, MS	[155]	0.15	0.88
43	Parathion	Lettuce	Davis, CA	[156]	1.75	1.92
44	Parathion	Peach	Modesto, CA	[157]	1.69	1.17
45	Parathion	Peach	Modesto, CA	[157]	1.88	1.30
46	Parathion	Peach	Wenatchee, WA	[158]	1.80	1.93
47	Parathion	Plum	Parlier, CA	[159]	1.49	0.89
48	Parathion	Potato	Biddinghuizen, Netherlands	[55]	0.63	1.05
49	Parathion	Spinach	Davis, CA	[160]	1.41	1.45

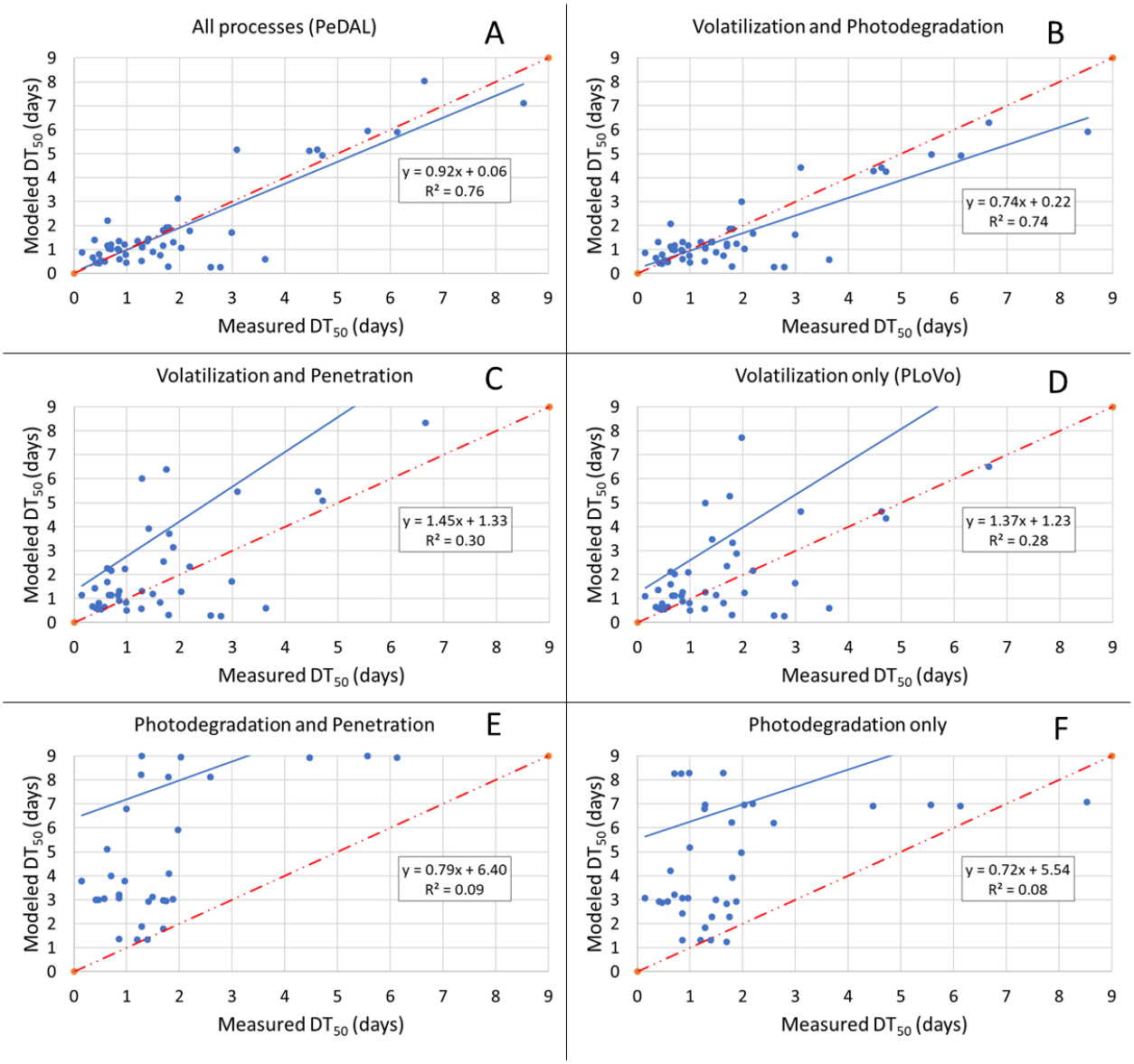

Figure A1. Evaluation graphs of modeled versus measured DT_{50} values using various combinations of dissipation processes

(A) Complete PeDAL model with all processes; (B) Volatilization and photodegradation; (C) Volatilization and penetration; (D) Volatilization only (PLoVo model); (E) Photodegradation and penetration; (F) Photodegradation only

Dashed lines represent the 1:1 line and solid lines display the line of best fit. In some cases, excluding processes resulted in several data points not reaching their DT_{50} after 14 days. In those instances, 14 days was used as the modeled value which means the fit would be even worse than what is reported for those graphs (C-F). The same scale was used for each graph for easier comparison.

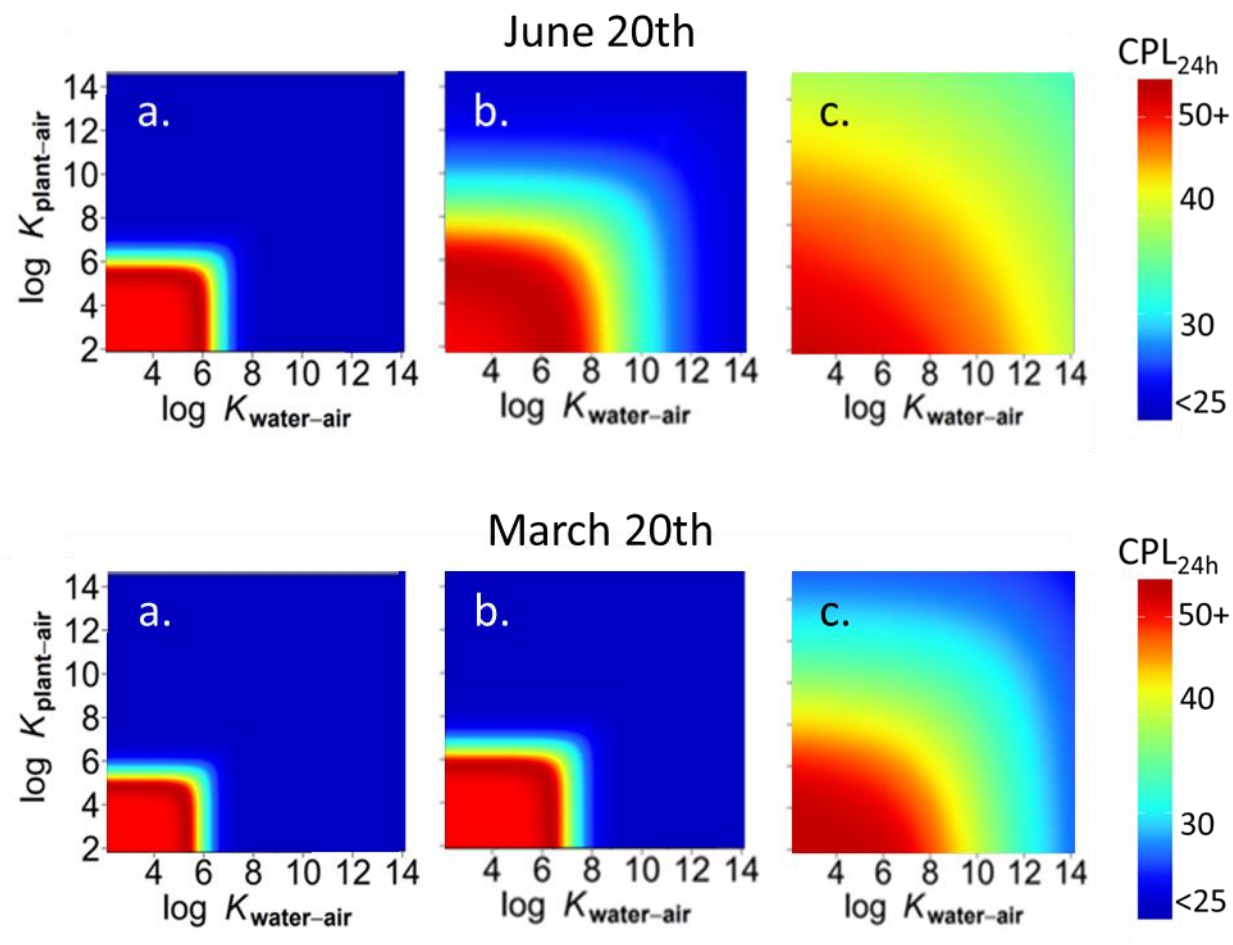

Figure A2. Chemical space diagrams

Two sets of chemical space diagrams showing CPL_{24h} values (%) for an application to a generic plant under two sets of meteorological conditions (Table A1) with the top panel representing conditions in June (also identical to Figure 5) and the bottom panel representing those in March. The hree levels of photodegradation are (a) slow photodegradation ($k_{photo(ref)}$=1.37x10^{-3} h^{-1} and I_{ref}=1000 W m^{-2}); (b) moderate photodegradation ($k_{photo(ref)}$=2.22x10^{-2} h^{-1} and I_{ref}=500 W m^{-2}); and (c) fast photodegradation ($k_{photo(ref)}$=2.90x10^{-2} h^{-1} and I_{ref}=320 W m^{-2}).

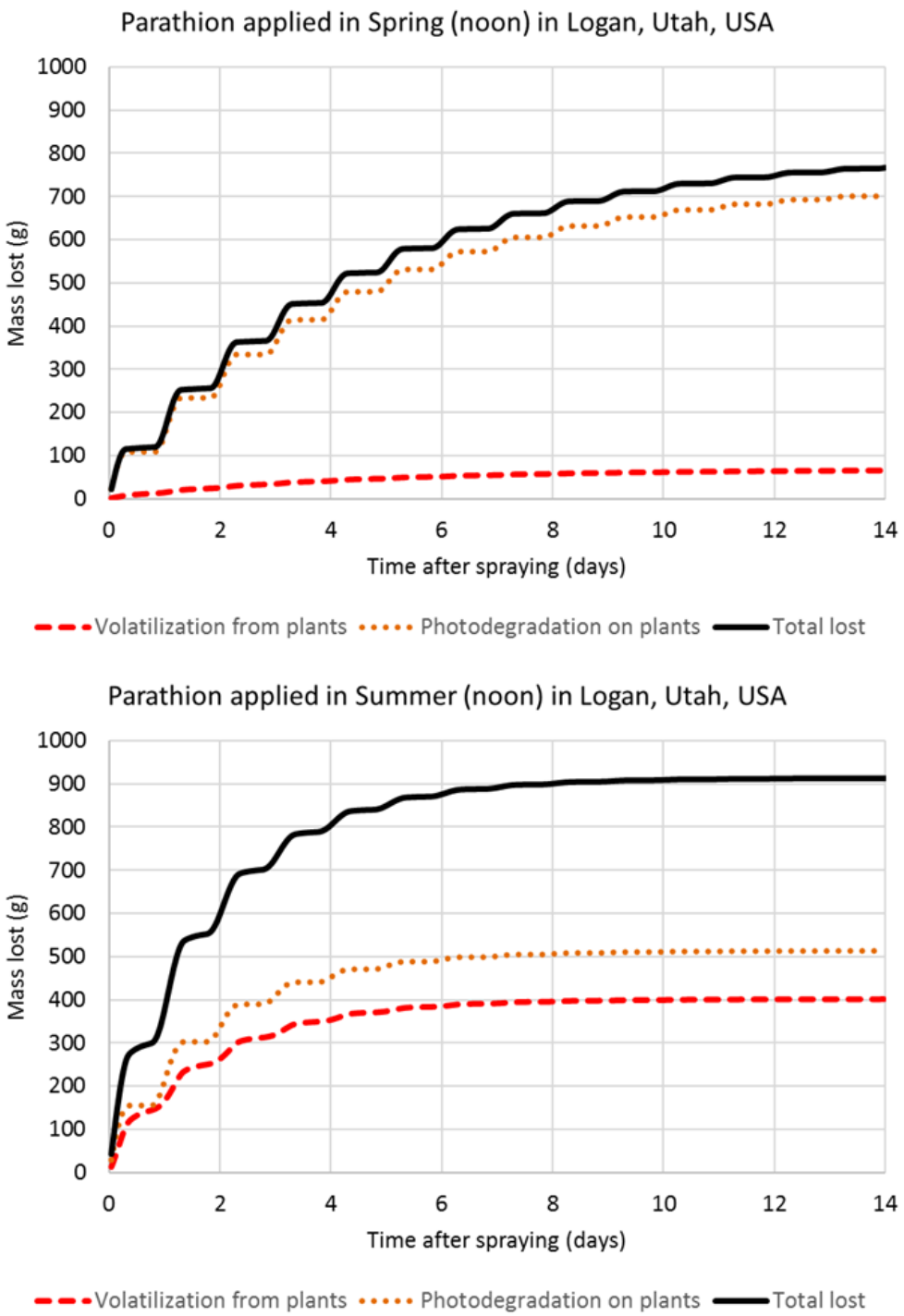

Figure A3. Pesticide loss contributions from individual processes for parathion applied to a clover crop under two sets of conditions in Logan, Utah, USA

Input parameters used for these scenarios are located in Table A8.

Table A11. Input parameters for modeled scenarios using lambda-cyhalothrin and indoxacarb

Input	Lambda-cyhalothrin scenario[75]		Ref.
	Site 1	Site 2	
Month	January	January	[75]
Day of month	15th	15th	*d*
Temperature (°C)	20	20	[162]
Wind speed (m/s)	1.5	1.5	[162]
Cloud coverage (%)	10	10	[161]
Relative Humidity (%)	69	69	[162]
Latitude	10.33°N	11. 50°N	*g*
Longitude	76.96°E	76.49°N	*g*
Time zone (+ is E of GMT)	+5	+5	*g*
Elevation (m)	1140	1150	*g*
Spray time (24-h clock)	12	12	*d*
%*I*	100	100	*d*
Leaf area index	4	4	*d*
Leaf length (m)	0.1	0.1	*d*
Leaf thickness (m)	0.000200	0.000200	*d*

Input	Indoxacarb scenario[77]	Ref.
Month	March	[77]
Day of month	15th	[d]
Temperature (°C)	23	[77]
Wind speed (m/s)	4.0	[162]
Cloud coverage (%)	10	[161]
Relative Humidity (%)	73	[77]
Latitude	30.04°N	[g]
Longitude	31.09°E	[g]
Time zone (+ is E of GMT)	+2	[g]
Elevation (m)	23	[g]
Spray time (24-h clock)	12	[d]
%*I*	100	[d]
Leaf area index	5	[164]
Leaf length (m)	0.2	[164]
Leaf thickness (m)	0.000267	[165]

[g]*indicates the latitude, longitude, or elevation wasn't reported in the paper so these values were estimated by using google.com*

[d]*indicates the default value listed in the List of Abbreviations was used because precise value couldn't be determined.*